Article

Synthesis, Crystal Structure, Characterization, and Catalytic Properties of TNU-9

Suk Bong Hong, Hyung-Ki Min, Chae-Ho Shin, Paul A. Cox, Stewart J. Warrender, and Paul A. Wright

J. Am. Chem. Soc., **2007**, 129 (35), 10870-10885• DOI: 10.1021/ja073109g • Publication Date (Web): 15 August 2007

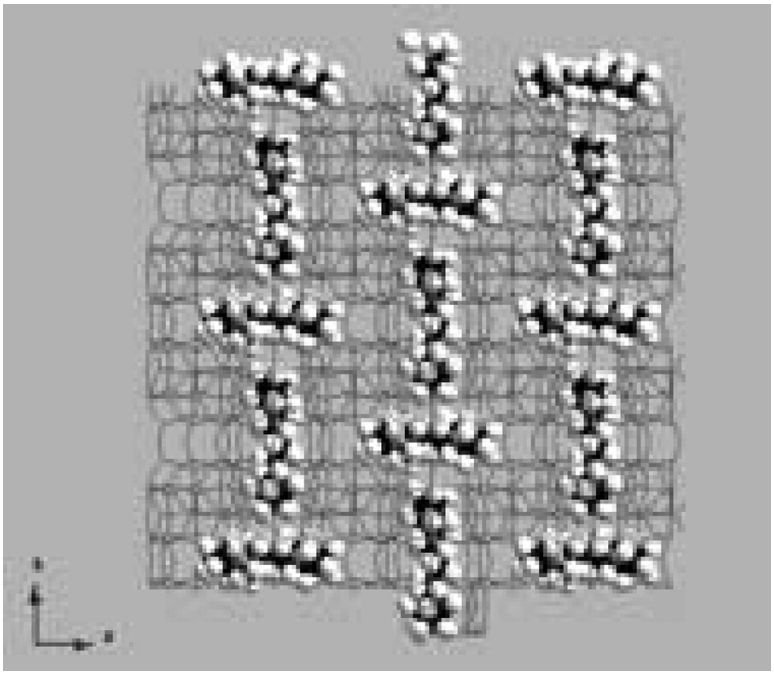

J|A|C|S
ARTICLES
Published on Web 08/15/2007

Synthesis, Crystal Structure, Characterization, and Catalytic Properties of TNU-9

Suk Bong Hong,*,† Hyung-Ki Min,‡ Chae-Ho Shin,‡ Paul A. Cox,§ Stewart J. Warrender,⊥ and Paul A. Wright⊥

Contribution from the School of Environmental Science and Engineering, POSTECH, Pohang 790-784, Korea, Department of Chemical Engineering, Chungbuk National University, Chungbuk 361-763, Korea, School of Pharmacy and Biomedical Science, University of Portsmouth, Portsmouth PO1 2DT, United Kingdom, and School of Chemistry, University of St. Andrews, St. Andrews, Fife KY16 9ST, United Kingdom

Received May 3, 2007; E-mail: sbhong@postech.ac.kr

Abstract: The synthesis, crystal structure, characterization, and catalytic properties of the novel medium-pore zeolite TNU-9 (framework type **TUN**), one of the most crystallographically complex zeolites known to date, are described. TNU-9 was found to crystallize under hydrothermal conditions at the expense of a lamellar precursor over a very narrow range of SiO_2/Al_2O_3 and $NaOH/SiO_2$ ratios and in the presence of 1,4-bis(*N*-methylpyrrolidinium)butane and Na^+ ions as structure-directing agents. A combination of molecular modeling and Rietveld refinement using synchrotron powder diffraction data confirms the proposed topology of as-made TNU-9 and suggests three or possibly four different sites for the organic within the complex pore structure. The proton form (H-TNU-9) of this new medium-pore zeolite exhibits exceptionally high hydrothermal stability, as well as very strong acidity. When compared to H-ZSM-5, H-MCM-22, H-mordenite, and H-Beta, H-TNU-9 displays unique shape selectivities for the acid-catalyzed reactions of monoaromatic hydrocarbons such as the disproportionation of toluene and the isomerization and disproportionation of *m*-xylene. In particular, for the isomerization of *m*-xylene, the ratio of isomerization to disproportionation increases steadily to values in excess of 50 with prolonged time on stream and a high *p*/*o* xylene ratio is observed in the products, achieving a value of ca. 6 after only a short time on stream. These results are rationalized on the basis of the unique pore topology of TNU-9.

1. Introduction

The use of zeolites as molecular sieves and catalysts is now well established in a wide variety of petrochemical and refining processes. However, keen interest remains in the search for novel zeolite structures, because of their capability to improve current catalysis and separation technologies and also to facilitate entirely new processes based on shape selectivity effects. In fact, the structural regime of this important class of microporous materials has been dramatically expanded over the past decade,[1] largely due to the continual progression of rational synthetic strategies.[2]

Our ongoing project on zeolite syntheses using linear diquaternary alkylammonium ions including aliphatic or cyclic moieties as structure-directing agents (SDAs) has revealed that the phase selectivity of the crystallization in the presence of such flexible organic cations is very sensitive to the Al content and the type and concentration of alkali cations in synthesis mixtures.[3−6] When some of these organic SDAs produce more than one zeolite structure, the occluded molecules were found to adopt distinct conformations that are closely related to the structural aspects of each zeolite host. This has led us to propose that the conformation control of organic SDAs with a high degree of flexibility and, when protonated, hydrophilicity by varying the concentrations of inorganic components in the aluminosilicate system could be an alternative strategy for the discovery of new structures.[6,7]

† POSTECH.
‡ Chungbuk National University.
§ University of Portsmouth.
⊥ University of St. Andrews.

(1) International Zeolite Association, Structure Commission, http://www.iza-structure.org.
(2) (a) Davis, M. E.; Zones, S. I. In *Synthesis of Porous Materials*; Occelli, M. L.; Kessler, H., Eds.; Marcel Dekker: New York, 1997; p 1. (b) Bu, X.; Feng, P.; Stucky, G. D. *Science* **1997**, *278*, 2080. (c) Villaescusa, L. A.; Camblor, M. A. *Recent. Res. Dev. Chem.* **2003**, *1*, 158. (d) Blackwell, C. S. et al. *Angew. Chem., Int. Ed.* **2003**, *42*, 1737. (e) Corma, A. In *Proceedings of the 14th International Zeolite Conference*; van Steen, E., Callanan, L. H., Claeys, M., Eds.; Document Transformation Technologies: Cape Town, 2004; p 25.
(3) (a) Lee, S.-H.; Shin, C.-H.; Hong, S. B. *Chem. Lett.* **2003**, *32*, 542. (b) Lee, S.-H.; Shin, C.-H.; Yang, D.-K.; Ahn, S.-D.; Nam, I.-S.; Hong, S. B. *Microporous Mesoporous Mater.* **2004**, *68*, 97.
(4) (a) Paik, W. C.; Shin, C.-H.; Hong, S. B. *Chem. Commun.* **2000**, 1609. (b) Lee, S.-H.; Lee, D.-K.; Shin, C.-H.; Paik, W. C.; Lee, W. M.; Hong, S. B. *J. Catal.* **2000**, *196*, 158. (c) Lee, S.-H.; Shin, C.-H.; Choi, G. J.; Park, T.-J.; Nam, I.-S.; Hong, S. B. *Microporous Mesoporous Mater.* **2003**, *60*, 237.
(5) (a) Han, B.; Lee, S.-H.; Shin, C.-H.; Cox, P. A.; Hong, S. B. *Chem. Mater.* **2005**, *17*, 477. (b) Han, B.; Shin, C.-H.; Nam, I.-S.; Hong, S. B. *Stud. Surf. Sci. Catal.* **2005**, *158*, 183.
(6) (a) Lee, S.-H.; Lee, D.-K.; Shin, C.-H.; Park, Y. K.; Wright, P. A.; Lee, W. M.; Hong, S. B. *J. Catal.* **2003**, *215*, 151. (b) Hong, S. B.; Lear, E. G.; Wright, P. A.; Zhou, W.; Cox, P. A.; Shin, C.-H.; Park, J.-H.; Nam, I.-S. *J. Am. Chem. Soc.* **2004**, *126*, 5817. (c) Hong, S. B. Korean Patent 480229, 2005.

10.1021/ja073109g CCC: $37.00

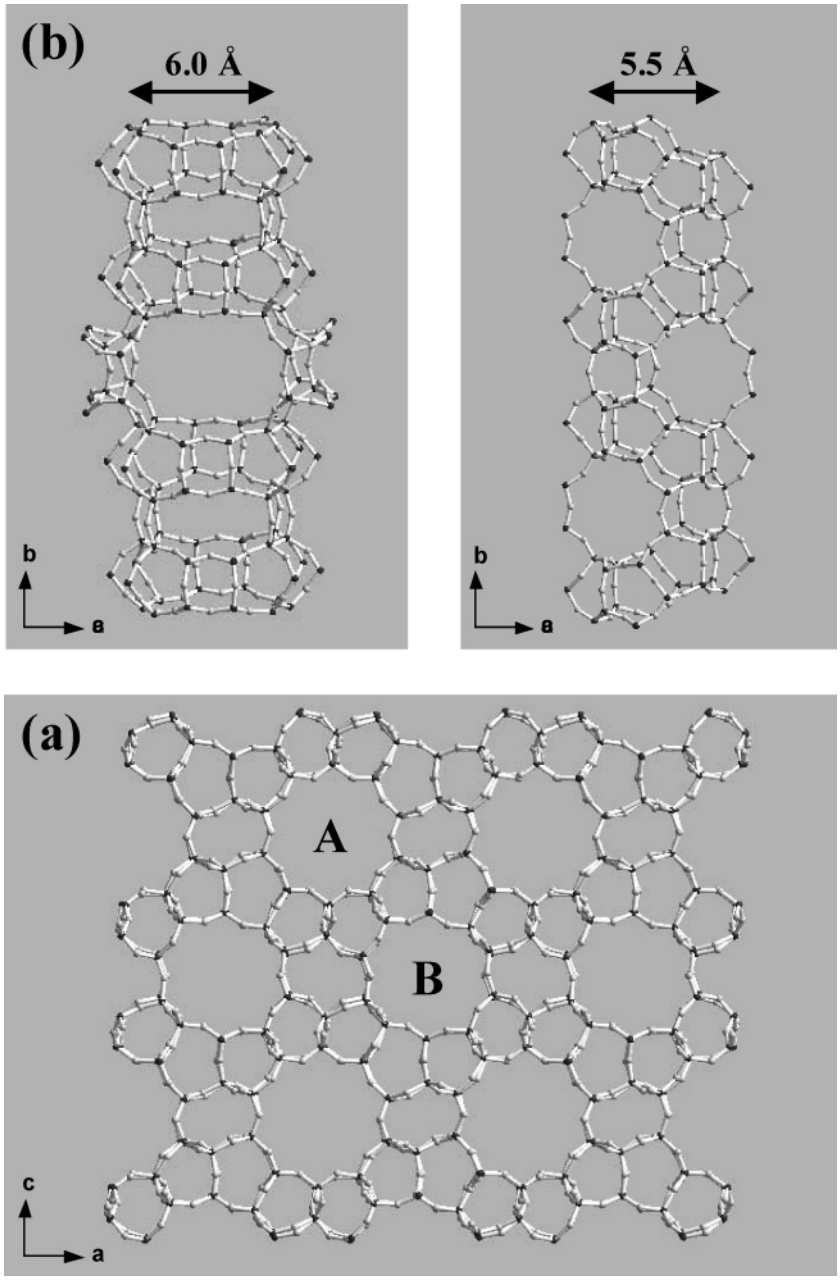

Figure 1. Framework structure of TNU-9: (a) the projection down the *b*-axis, showing the arrangement of the two wider and narrower 10-ring channels, labeled A and B, respectively, and (b) the internal surface of each of these two channels running parallel to the *b*-axis.

TNU-9 is a new high-silica zeolite that, using the above strategy, we have previously synthesized in the presence of a flexible diquaternary cation, 1,4-bis(*N*-methylpyrrolidinium)-butane as an organic SDA and Na^+.[6b] Recently, the framework structure of this zeolite has been solved through the combined use of powder diffraction and electron microscopy.[8] TNU-9 is one of the most complex zeolites known, possessing 24 crystallographically distinct tetrahedral sites (T-sites) with equal populations in its monoclinic unit cell. Figure 1 illustrates the projection of the TNU-9 framework down the *b*-axis and indicates the arrangement of the two distinct 10-ring (5.2 × 6.0 and 5.1 × 5.5 Å) channels labeled A and B, respectively, together with the internal surface of each channel. The shorter bridging sections at their narrowest by 10-rings (5.4 × 5.5 Å) between these two 10-ring channels are found to connect either between two of the narrower (B) channels or between a narrower (B) channel and a wider (A) one, as shown in Figure 2. Very recently, the structure of TNU-9 (*C*2/*m*; $a = 27.8449$ Å, $b = 20.0150$ Å, $c = 19.5965$ Å, $\beta = 93.000°$) has been given the code **TUN** by the International Zeolite Association.[1]

In the present contribution we describe the synthetic details of TNU-9, its crystal structure in the as-made form determined by combining high-resolution synchrotron powder diffraction and computer simulation data, and the physicochemical properties of this new medium-pore zeolite that have been characterized extensively by powder X-ray diffraction, elemental and thermal analyses, scanning electron microscopy, N_2 and Ar

(7) (a) Paik, W. C.; Shin, C.-H.; Lee, J. M.; Ahn, B. J.; Hong, S. B. *J. Phys. Chem. B* **2001**, *105*, 9994. (b) Han, D.-Y.; Woo, A. J.; Nam, I.-S.; Hong, S. B. *J. Phys. Chem. B* **2002**, *106*, 6206.
(8) Gramm, F.; Baerlocher, Ch.; McCusker, L. B.; Warrender, S. J.; Wright, P. A.; Han, B.; Hong, S. B.; Liu, Z.; Ohsuna, T.; Terasaki, O. *Nature* **2006**, *444*, 79.

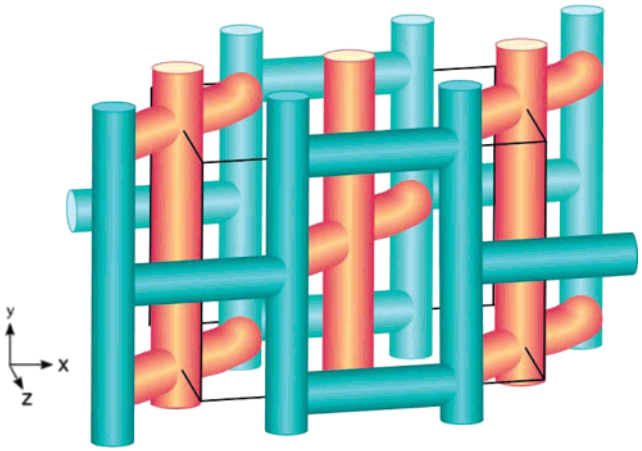

Figure 2. Schematic drawing of the three-dimensional channel system of TNU-9: channels A in orange and channels B in green. Adapted from ref 8.

adsorption, multinuclear MAS NMR, and IR measurements of adsorbed pyridine. We also report the catalytic properties of TNU-9 for the disproportionation of toluene and the isomerization and disproportionation of *m*-xylene. The catalytic results are compared to those obtained from several other zeolites with well-known structures that are widely used in current catalytic processes.

2. Experimental Section

2.1. Synthesis. The divalent 1,4-bis(*N*-methylpyrrolidinium)butane (1,4-MPB) cation was prepared, purified, and characterized as previously described.[6b]

Zeolite syntheses using 1,4-MPB were performed using gels prepared by combining NaOH (50% aqueous solution, Aldrich), $Al(NO_3)_3 \cdot 9H_2O$ (98%, Junsei), fumed silica (Aerosil 200, Degussa), and deionized water. The final gel composition was $4.5(1,4\text{-MPB}) \cdot x Na_2O \cdot y Al_2O_3 \cdot 30SiO_2 \cdot 1200H_2O$, where x and y are varied between $5.0 \leq x \leq 17.0$ and $0 \leq y \leq 2.0$, respectively. When necessary, NaOH was replaced by the equivalent amount of $LiOH \cdot H_2O$ (98%, Aldrich) or KOH (45% aqueous solution, Aldrich). Also, a small amount (2 wt % of the silica in the gel) of seed crystals was added to the synthesis mixture. The seed crystals used here were the standard TNU-9 sample in the as-made form that was previously obtained according to the original synthetic procedure.[6b] After being stirred at room temperature for 1 day, the final synthesis mixture was transferred to Teflon-lined 45-mL autoclaves and heated at 433 K, with or without stirring (100 rpm) under autogenous pressure, for 1−28 days. For comparison, some syntheses were carried out using 1,4-dibromobutane (1,4-DBB, 99%, Aldrich) and 1-methylpyrrolidine (1-MP, 97%, Aldrich) as organic SDAs, instead of 1,4-MPB, that are precursors of the diquaternary salt. In this set of synthesis experiments, the gel composition was fixed to $4.5(1,4\text{-DBB}) \cdot x(1\text{-MP}) \cdot 11Na_2O \cdot 0.5Al_2O_3 \cdot 30SiO_2 \cdot 1200H_2O$, where x is 9.0 or 13.5. The solid products were recovered by filtration, washed repeatedly with water, and then dried overnight at room temperature.

As-made TNU-9 was calcined under flowing air at 823 K for 8 h to remove the occluded organic SDA. The calcined sample was then refluxed twice in 1.0 M NH_4NO_3 solutions for 6 h followed by calcination at 823 K for 4 h in order to obtain its proton form (i.e., H-TNU-9). Dealumination was carried by a two-step procedure. First, 3.0 g of H-TNU-9 was refluxed in 100 mL of 6.0 N nitric acid solutions for 18 h. Then, 2.0 g of the acid-treated sample were placed inside an Inconel reactor in a vertical tube furnace. The reactor was purged with dry air (100 $mL \cdot min^{-1}$), and its temperature was increased at a heating rate of 3 $K \cdot min^{-1}$ to a final temperature of 1123 K. After replacing the air flow by 100% steam (100 $mL \cdot min^{-1}$), the reactor was kept at this temperature for 3 days. Finally, the steamed solid was allowed to return back to room temperature under flowing air.

For catalytic comparison, zeolite MCM-22 (**MWW**) with Si/Al = 16.8 was prepared and converted to its proton form following the procedures given elsewhere.[9] In addition to this zeolite, NH_4-ZSM-5 (**MFI**) with Si/Al = 13.5, H-mordenite (**MOR**) with Si/Al = 16.7, and NH_4-beta (***BEA**) with Si/Al = 12.5 were obtained from ALSI-PENTA-Zeolithe, Tosoh, and PQ, respectively.

2.2. Modeling and Structural Analysis of As-Made TNU-9. Computer simulations and structural analysis of the as-made material were performed to assess the structure-directing role of the diquaternary 1,4-MPB cation in the crystallization of TNU-9. A Monte Carlo simulated annealing (MC-SA) approach[10] was employed to predict the energy-minimized locations of organic SDA molecules inside the TNU-9 framework. All calculations were performed on a Silicon Graphics R10000 machine using the program Discover.[11] The framework was held fixed during the calculations and was modeled as a fully siliceous structure. Short-range forces were calculated using the CVFF forcefield, with partial charges included only on the SDA molecules. Initially, one molecule was docked into a single unit cell of the TNU-9 framework. This simulation box was repeated using periodic boundary conditions in order to represent an infinite 3-D structure. Simulated annealing for 2000 time steps of 1×10^{-15} s at temperatures of 750, 500, 300, and 200 K were performed prior to a final energy minimization using a combination of conjugate gradient and va09a algorithms until the maximum derivative was less than 0.08 $kJ \cdot Å^{-1}$. Further addition of SDA molecules one at a time to the calculation until no further improvement in the binding energy per SDA was obtained.

The high-resolution powder X-ray diffraction (XRD) pattern for as-made TNU-9 was collected at room temperature on the Swiss-Norwegian Beamline at the ESRF (Grenoble, France) using monochromated X-rays (λ = 0.500 07 Å). The sample, loaded into a 1.0 mm glass capillary, was spun for better powder averaging, and the XRD data were obtained with a step size of 0.01° for a scan time of 6 s per step over the range $1° \leq 2\theta \leq 30°$. Typically, as-made TNU-9 contains a trace amount of unknown impurity (probably zeolite NU-87 with the **NES** topology). Thus, reflections due to this impurity phase were excluded from the Rietveld structure refinement, which was conducted in the program GSAS[12] over the range $1-28°\theta$. Refinement of a starting model, comprising the framework of TNU-9[8] and including organic SDA molecules in their energy minimized positions, was performed against the XRD profile using the Rietveld method.[12] To describe the peak shape, a psuedo-Voigt function[13] was used together with a linearly interpolated background. The framework was modeled as completely siliceous. Si−O bond lengths were constrained within the GSAS program to be 1.61 Å (σ = 0.005 Å), and O−O distances within the same tetrahedra were constrained to be 2.63 Å (σ = 0.01 Å). These constraints were maintained throughout the course of the refinement. Organic SDA positions were initially fixed at their energy minimized locations within the TNU-9 pores determined via computer modeling studies and then allowed to refine, with restraints. Isotropic displacement parameters of all Si atoms were constrained to be equal, as were those of all O atoms and those of all SDA atoms.

2.3. Characterization. Phase identity and purity of the solid products were checked by powder XRD patterns using a Rigaku 2500H diffractometer with Cu Kα radiation. The crystallinity of a series of the products obtained by heating a synthesis mixture with the optimized

(9) (a) Corma, A.; Corell, C.; Perez-Pariente, J. *Zeolites* **1995**, *15*, 2. (b) Mochida, I.; Eguchi, S.; Hironaka, M.; Nagao, S.; Sakanishi, K.; Whitehurst, D. D. *Zeolites* **1997**, *18*, 142.
(10) Stevens, A. P.; Gorman, A. M.; Freeman, C. M.; Cox, P. A. *J. Chem. Soc., Faraday Trans.* **1996**, *92*, 2065.
(11) Discover version 99.1, Accelrys, San Diego, USA.
(12) Larson, A.; von Dreele, R. B. *General Structure Analysis System GSAS*; Los Alamos National Laboratory: Los Alamos, NM, 1994.
(13) Hastings, J. B.; Thomlinson, W.; Cox, D. E. *J. Appl. Crystallogr.* **1984**, *17*, 85.

gel composition for TNU-9 formation at 433 K for different periods (1−28 days) of time was determined by comparing the area of the most intense X-ray peak around $2\theta = 22.8°$, corresponding to the (151) reflection of this new medium-pore structure, with that of the standard sample described above. While no special care was taken to eliminate preferred orientation effects on the XRD pattern of the respective product crystals, exactly the same amount of sample was loaded in the sample holder for all measurements. Elemental analysis for Si, Al, and Na was carried out by a Jarrell-Ash Polyscan 61E inductively coupled plasma (ICP) spectrometer in combination with a Perkin-Elmer 5000 atomic absorption spectrophotometer. The C, H, and N contents of selected samples were analyzed by using a Carlo Erba 1106 elemental organic analyzer. Thermogravimetric analyses (TGA) were performed in air on a TA Instruments SDT 2960 thermal analyzer, where the exothermic weight loss related to the combustion of organic species or of coke deposits formed during the test reactions performed in this study was further confirmed by differential thermal analyses (DTA) using the same analyzer. Crystal morphology and size were determined by a JEOL JSM-6300 scanning electron microscope (SEM). The Ar and N_2 sorption experiments were performed on a Micromeritics ASAP 2010 analyzer.

$^1H-^{13}C$ CP MAS NMR spectra at a spinning rate of 4.5 kHz were measured on a Bruker Avance 500 spectrometer at a ^{13}C frequency of 125.767 MHz with a $\pi/2$ rad pulse length of 5.0 μs, a contact time of 1 ms, and a recycle delay of 5 s. Typically, 6000 pulse transients were accumulated. ^{29}Si MAS NMR spectra at a spinning rate of 10.0 kHz were measured at a ^{29}Si frequency of 99.352 MHz. The spectra were obtained with an acquisition of ca. 1000 pulse transients, which were repeated with a $\pi/2$ rad pulse length of 5.0 μs and a recycle delay of 30 or 60 s. The ^{13}C and ^{29}Si chemical shifts are referenced to TMS. ^{27}Al MAS NMR spectra at a spinning rate of 11.0 kHz were recorded at a ^{27}Al frequency of 130.336 MHz, with a $\pi/20$ rad pulse length of 0.5 μs, a recycle delay of 1 s, and an acquisition of about 1000 pulse transients. The ^{27}Al chemical shifts are referenced to an $Al(H_2O)_6^{3+}$ solution.

The IR spectra in the OH region were measured on a Nicolet 360 FT-IR spectrometer using self-supporting zeolite wafers of approximately 15 mg (1.3-cm diameter). Prior to IR measurements, the zeolite wafers were dehydrated at 723 K under vacuum to a residual pressure of 10^{-5} Torr for 2 h inside a home-built IR cell with CaF_2 windows. For IR spectroscopy with adsorbed pyridine, the activated self-supporting wafer was contacted with a pyridine-loaded flow of dry He at 373 K for 0.5 h, evacuated (10^{-3} Torr) at the same temperature for 1 h to remove physisorbed pyridine, and then heated at different temperatures. After each desorption step, the concentrations of Brönsted and Lewis acid sites were determined from the intensities of the IR bands around 1550 and 1450 cm^{-1}, respectively, using the equations of Emeis.[14]

2.4. Catalysis. All the catalytic experiments were conducted under atmospheric pressure in a continuous-flow apparatus with a fixed-bed microreactor. Prior to the experiments, the catalyst was routinely activated under flowing He (50 $cm^3 \cdot min^{-1}$) at 773 K for 2 h and kept at the desired temperature to establish a standard operating procedure allowing time for the product distribution to stabilize. In the disproportionation of toluene, a reactant stream with an N_2/toluene molar ratio of 5.1 was fed into a quartz reactor containing 0.2 g of zeolite catalyst at 573 K. The total gas flow at the reactor inlet was kept constant at 30 $cm^3 \cdot min^{-1}$ to give a weight hourly space velocity (WHSV) of 7.2 h^{-1}. The isomerization and disproportionation of *m*-xylene were carried out at 623 K with an N_2/*m*-xylene molar ratio of 4.0. Because of notable differences in the catalytic activity of zeolites employed here, the amount of catalyst and the molar flow of *m*-xylene at the reactor inlet were adapted to obtain the desired level of conversion. The products of both reactions were analyzed on-line in a Varian CP-3800 gas chromatograph equipped with a 25-m long CP-Chirasil-Dex CB capillary column and a flame ionization detector. Under the conditions described above, 5 min on stream was found to be the lowest value at which the reactant pressure in each reaction stream could be considered as constant from the sum of the surface areas of the gas chromatograph peaks. To account for the deactivation of the zeolite catalysts due to coke formation and their different decay rates, therefore, initial reaction rates and product distributions were calculated by extrapolating the time-dependent data to zero time on stream.

(14) Emeis, C. A. *J. Catal.* **1993**, *141*, 347.

Table 1. Representative Synthesis Conditions and Results[a]

run no.	gel composition SiO_2/Al_2O_3	gel composition $NaOH/SiO_2$	product[b]
1	60	0.73	TNU-9
2[c]	60	0.73	amorphous
3	15	0.73	analcime + (TNU-9)
4	30	0.73	mordenite + TNU-9
5	40	0.73	TNU-9
6	120	0.73	quartz + (TNU-9)
7	∞	0.73	MCM-47
8[d]	∞	0.73	MCM-47
9	60	1.00	TNU-10
10	60	0.87	TNU-9 + IM-5
11	60	0.60	ZSM-12
12	60	0.47	ZSM-12
13	60	0.73[e]	D + (ZSM-12)
14	60	0.73[f]	amorphous
15[g]	60	0.73	TNU-9
16[h]	60	0.73	TNU-9

[a] The oxide composition of the synthesis mixture is 4.5(1,4-MPB)·$x$$Na_2O$·$y$$Al_2O_3$·30$SiO_2$·1200$H_2O$, where x and y are varied between $7.0 \leq x \leq 15.0$ and $0.0 \leq y \leq 2.0$, respectively. Crystallization was performed under rotation (100 rpm) at 433 K for 14 days, unless otherwise stated. [b] The product appearing first is the major phase, and the product obtained in a trace amount is given in parentheses. D is an unknown but probably dense phase. [c] Run performed under static conditions. [d] Run performed after adding a small amount (2 wt % of the silica in the gel) of the previously prepared TNU-9 sample as seeds to the synthesis mixture. [e] $LiOH/SiO_2$ ratio. [f] KOH/SiO_2 ratio. [g] Run performed using a gel with the oxide composition 4.5(1,4-DBB)·9.0(1-MP)·11Na_2O·0.5Al_2O_3·30SiO_2·1200H_2O at 433 K for 10 days. [h] Run performed using a gel with the oxide composition 4.5(1,4-DBB)·13.5(1-MP)·11Na_2O·0.5Al_2O_3·30SiO_2·1200H_2O at 433 K for 6 days.

3. Results and Discussion

3.1. Synthesis. Table 1 lists the representative products obtained using 1,4-MPB as an organic SDA from synthesis mixtures with different oxide compositions under the conditions described above. In each case, the phases listed were the only ones obtained in repeated trials. The synthesis results in Table 1 reveal that the crystallization of TNU-9 in the presence of 1,4-MPB is possible only from synthesis mixtures with a very narrow range of SiO_2/Al_2O_3 and $NaOH/SiO_2$ ratios. When the $NaOH/SiO_2$ ratio in the gel is fixed to 0.73, for example, the SiO_2/Al_2O_3 ratio yielding TNU-9 was found to be in the range 40−60. When using sodium aluminosilicate gels with $SiO_2/Al_2O_3 \leq 30$, however, we always obtained analcime (**ANA**) or mordenite as the major phase. In addition, MCM-47, a pure-silica layered material composed of ferrierite (**FER**) sheets,[15] was the phase that crystallized from the Al-free synthesis mixture. We should note here that no changes in the product were observed, even though a small amount (2 wt % of the silica in the gel) of the previously prepared TNU-9 sample was added as seeds to this synthesis mixture.

(15) (a) Valyocsik, E. W. U.S. Patent 5068096, 1991. (b) Burton, A.; Accardi, R. J.; Lobo, R. F.; Falcioni, M.; Deem, M. W. *Chem. Mater.* **2000**, *12*, 2936.

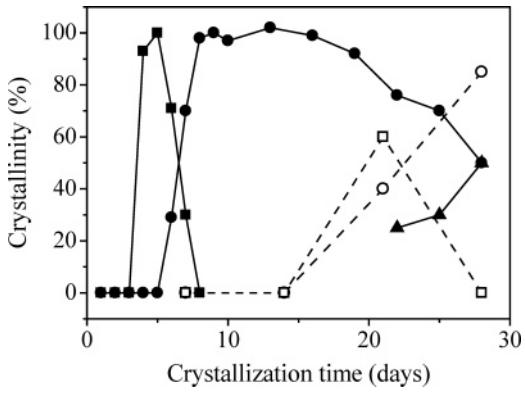

Figure 3. Crystallinity of TNU-9 (●) as a function of crystallization time from the optimized oxide composition ($SiO_2/Al_2O_3 = 60$ and $NaOH/SiO_2 = 0.73$) at 433 K under rotation (100 rpm). The closed squares and triangles indicate MCM-22(P) and quartz, respectively. The open squares and circles indicate MCM-22(P) and TNU-9 obtained under static conditions, respectively.

When the initial SiO_2/Al_2O_3 ratio in the synthesis mixture is fixed to 60, on the other hand, ZSM-12 (**MTW**) with the one-dimensional 12-ring pore system was the phase formed from synthesis mixtures with $NaOH/SiO_2 \leq 0.60$. In contrast, the synthesis using aluminosilicate gels with $NaOH/SiO_2 = 0.87$ yielded a mixture of TNU-9 and IM-5 (**IMF**), where the former was the major phase. It is interesting to note that the synthesis of IM-5, a new medium-pore, high-silica zeolite whose structure has very recently been solved,[16] normally includes the use of 1,5-bis(*N*-methylpyrrolidinium)pentane (1,5-MPP), a slightly longer diquaternary cation than 1,4-MPB, as an organic SDA.[6a,17] A further increase of the $NaOH/SiO_2$ ratio in the gel to 1.00 led to the crystallization of TNU-10, a high-silica **STI** zeolite, as reported in our previous work.[6b] Table 1 also shows that the replacement of NaOH with the equivalent amount of LiOH or KOH under the conditions where the crystallization of TNU-9 proved to be highly reproducible did not give this new medium-pore zeolite, revealing the strong influence of the type of alkali metal cations on the product selectivity in the 1,4-MPB-mediated synthesis of zeolites. It thus appears that there is a specific level of Na^+ ions in the synthesis mixture, together with a reasonable amount of lattice charge, in the crystallization of TNU-9 using 1,4-MPB. In our view this may make it possible to vary the conformation of 1,4-MPB within the gels of a particular range of oxide compositions and so to give any of the eight zeolitic phases which can be synthesized using the same organic SDA (i.e., 1,4-MPB),[6b] because the type of the conformation of such a flexible organic species dominant at zeolite crystallization conditions should be greatly affected by the nature and extent of interactions between the organic and inorganic components in synthesis mixtures.

Figure 3 shows the crystallization kinetics of TNU-9 from the optimized gel composition ($SiO_2/Al_2O_3 = 60$ and $NaOH/SiO_2 = 0.73$) at 433 K under rotation (100 rpm). Unexpectedly, a lamellar precursor of MCM-22, frequently referred as MCM-22(P), was the phase that first crystallized under the conditions described above (Supporting Information Figure 1S). TNU-9 then began to grow rapidly at the expense of MCM-22(P) and fully crystallized after about 8 days of heating. This implies that MCM-22(P) has a lower activation for nucleation and/or crystallization than TNU-9, making its formation kinetically favored, but it is thermodynamically less stable, readily transforming in situ into the latter phase in the crystallization medium. Given its layered nature, on the other hand, the framework density (FD), defined as the number of T-atoms per 1000 Å^3, of MCM-22(P) cannot be larger than that (15.9) of the fully connected three-dimensional MCM-22 structure. Because TNU-9 has a larger FD value (17.6) than MCM-22,[1] the formation of this more condensed phase is expected to proceed by Ostwald ripening through a dissolution/recrystallization. It is interesting to note here that the MCM-22(P) material synthesized in the presence of hexamethyleneimine, a well-known organic SDA for this layered phase, transforms into ZSM-35 (**FER**), when heated with prolonged time in the crystallization medium.[9] Since 1,4-MPB yields MCM-22(P) and TNU-9 in certain high-silica synthesis conditions and a lamellar precursor of ferrierite (i.e., MCM-47) in the absence of Al (Table 1), the reason 1,4-MPB−MCM-22(P) transform to TNU-9 rather than to ZSM-35 may likely be related to the energetic difference at synthesis temperatures between 1,4-MPB−TNU-9 and 1,4-MPB−MCM-47, depending on their Al content. Figure 3 also shows that TNU-9 is stable for an additional 10 days of heating in the crystallization medium but ultimately transforms into quartz, revealing its metastable nature in the crystallization conditions. When the synthesis is performed under static conditions, however, a crystallization time of more than 4 weeks was required to fully crystallize TNU-9. This indicates that homogeneous mixing of the synthesis mixture at the crystallization temperature is not a critical factor governing the synthesis of TNU-9, although it speeds up the crystallization.

The synthesis results presented so far reveal that the structure-directing ability of 1,4-MPB is not robust enough to dominate over the impact of inorganic gel chemistry. However, we found that the presence of this flexible diquaternary cation in the synthesis mixture is also prerequisite for the crystallization of TNU-9 even under conditions where the gel composition ($SiO_2/Al_2O_3 = 60$ and $NaOH/SiO_2 = 0.73$) is optimized, suggesting some degree of specificity in its structure-directing properties. To further confirm this, we replaced 1,4-MPB in the aluminosilicate gel with the optimized oxide composition by its specific precursors (e.g., 1,4-DBB and 1-MP) and performed zeolite syntheses while keeping all other parameters constant. MCM-22(P) was the phase crystallized in the presence of 1,4-DBB and 1-MP with a molar ratio of 1:2 after 7 days of heating at 433 K. As in the case of using 1,4-MPB as an organic SDA, in addition, fully crystalline TNU-9 was obtained after an additional 3 days of heating in the crystallization medium. Since the use of either 1,4-DBB or 1-MP as an SDA always gave mordenite even under the optimized conditions for TNU-9 formation, it is not difficult to infer that 1,4-DBB and 1-MP probably react themselves to form 1,4-MPB in situ, first directing the synthesis of MCM-22(P) and then yielding TNU-9, as will be evidenced below. This tempted us to consider the crystallization of TNU-9 as the successful result of the cooperative structure-directing effects of 1,4-MPB and inorganic components (i.e., Na^+ and Al) with a particular narrow range of concentrations. However, the actual situation appears to be more complex, since the crystallization time was reduced from

(16) Baerlocher, Ch.; Gramm, F.; Massüger, L.; McCusker, L. B.; He, Z.; Hovmöller, S.; Zou, X. *Science* **2007**, *315*, 1113.
(17) (a) Benazzi, E.; Guth, J. L.; Rouleau, L. PCT WO 98/17581, 1998. (b) Corma, A.; Chica, A.; Guil, J. M.; Llopis, F. J.; Mabilon, G.; Perdigon-Melon, J. A.; Valencia, S. *J. Catal.* **2000**, *189*, 382.

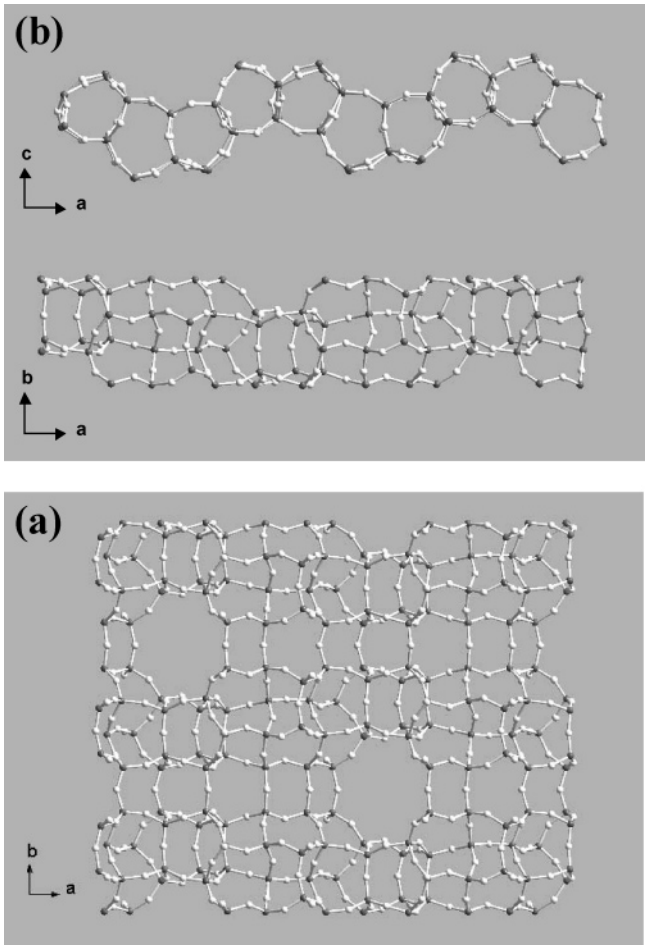

Figure 4. The (a) silicate sheet in TNU-9 and (b) views of its chain running along the *a*-axis, viewed down the *b*- (top) and *c*- (bottom) axes.

10 to 6 days when adding 1,4-DBB and 1-MP with a molar ratio of 1:3 to the synthesis mixture (Table 1). Thus, we might suspect the beneficial effect of small organic additives in the crystallization of TNU-9 (see below).

3.2. Structure-Directing Role of the Organic in TNU-9 Crystallization. Molecular simulation in symmetry *P*1 predicts a maximum filling of eight 1,4-MPB molecules per unit cell. These include four different organic SDA positions with a four more sites related to these by unit cell displacements of (0.5, 0.5, 0), resulting from the framework C-centering. The SDA positions are best discussed in terms of the channels and cages within the framework. Although very complex crystallographically, the framework of TNU-9 may be regarded as being built from only one single type of chain composed of 4-, 5-, and 6-rings. As shown in Figure 4, the chains extend along the *a*-axis and are linked into sheets in the *ab* plane via T−O−T linkages across mirror planes that are perpendicular to the *b*-axis. These sheets, which are asymmetric in that their two faces are different, contain 10-ring openings that are ultimately responsible for the perpendicular connectivity between the wider channels A and narrower channels B (Figure 2). The sheets link along the *c*-axis to form the complete structure: each sheet is related to its neighbor by inversion (and 2-fold axes running down the center of the A and B channels). Although each sheet is identical, due to their asymmetry, there are two types of intersheet region and therefore two different channels. Because of the asymmetry of

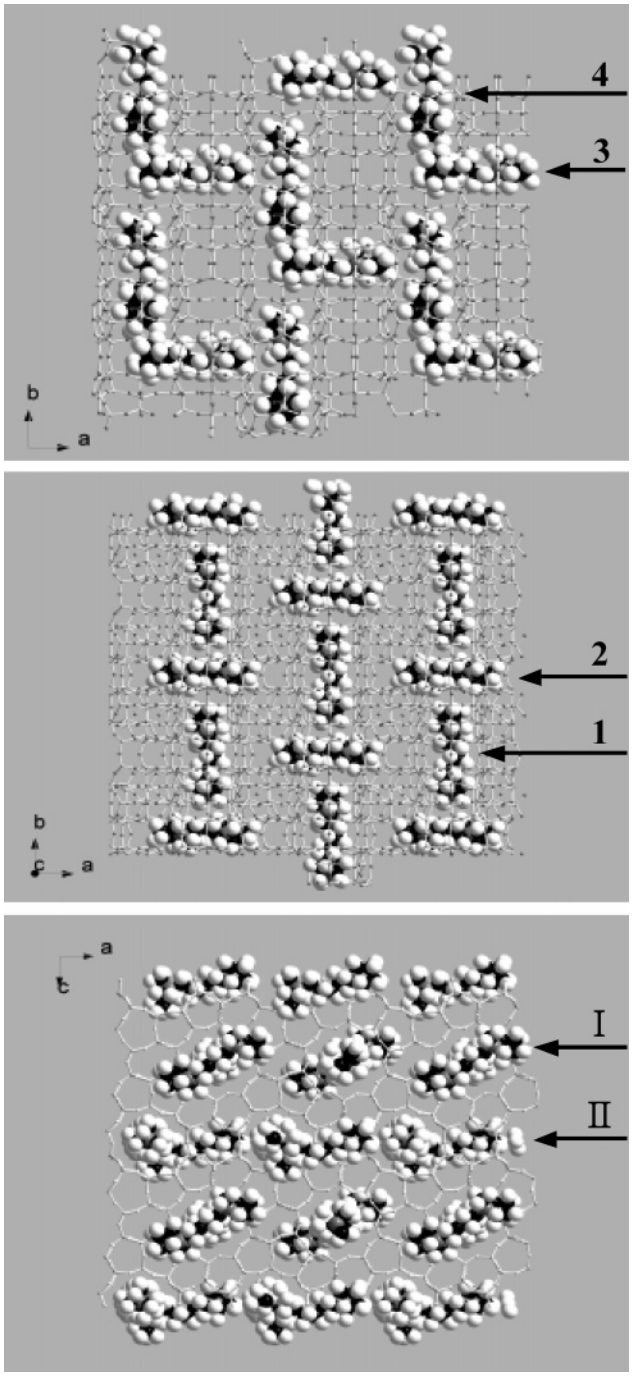

Figure 5. Two intersheet regions (bottom) in the TNU-9 framework and four distinct positions (middle and top) of the occluded 1,4-MPB molecules as determined by modeling studies.

the sheets, the different sides of two sheets cannot straightforwardly be linked.

Figure 5 shows the four distinct 1,4-MPB positions in terms of their location within the intersheet regions of the TNU-9 framework, as determined by the energy minimization calculations. The two different intersheet regions are denoted I and II, respectively. Two different SDA positions were determined in each of the two intersheet regions. In intersheet region I, the diquaternary cations are arrayed head-to-middle-to-head, going along channel A. There are two clearly defined sites for SDA molecules within this area of the structure: one along the channel A (labeled **1**), and the second (labeled **2**) within "cages"

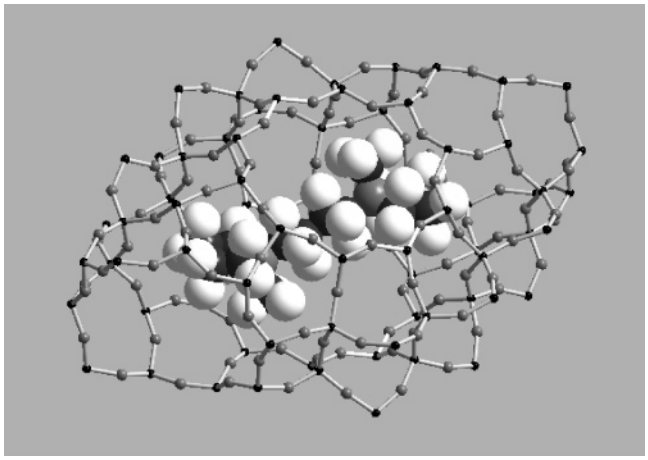

Figure 6. Energy-minimized conformation of the 1,4-MPB molecule within the large cage limited by the main channel A down the *b*-axis and by the short bridging 10-ring channel in the third direction.

Table 2. Distinct Positions and Nonbonded Energies for 1,4-MPB Ions within the TNU-9 Framework

position ID	SDA location	nonbonded energy, kJ·(mol SDA)$^{-1}$
1	intersheet region I, along channel A	−122.8
2	intersheet region I, in a cage and with the molecular lying perpendicular to channel A	−140.2
3	intersheet region II, in short channel sections linking the channel B	−31.8
4	intersheet region II, along the channel B	−111.3

where the main channel A is intersected by the shorter bridging 10-ring channel, as shown in Figure 6. Operation of the symmetry of the framework exerted little influence on the position of these organic molecules since they are located about twofold axes and on mirror planes.

Figure 5 also shows that, in intersheet region II, pore space could again be filled to a high degree by the organic SDA molecules in two positions, labeled **3** and **4**. While position **4** lies along channel B, position **3** is in the bridging channel section between B channels. There does not seem to be enough space for the molecule in position **3** to be fully extended, and hence this position has a less favorable nonbonded energy. If the symmetry operations of the framework are applied to positions **3** and **4**, we found that those running along channel B could be at several heights in the unit cell and that those in the short bridging channel sections could be displaced closer to either of the connected channels B, depending on the position of the molecules in channel B. In this second intersheet region, SDA molecules show both head-to-head and head-to-middle arrangements. Thus, the arrangement in Figure 5 is one of a symmetry related set that all show this general motif. It is also remarkable that, since none of the SDA molecules run through the framework sheets, connectivity between intersheet regions is not preprogrammed by the position of molecules and would appear, in that sense, to be fortuitous. The nonbonded energies for each of the four unique SDA positions within the intersheet regions of the TNU-9 framework, calculated for situations where the isolated molecules in each of the positions were simulated, are given in Table 2. All values were calculated to be negative. However, we note that while the values for positions **1**, **2**, and **4** are similar to one another, the nonbonded energy for position **3** is significantly smaller in magnitude, suggesting less favorable interactions in this position.

In order to assess the modeling predictions, Rietveld refinement of the synchrotron diffraction data for as-made TNU-9 was performed in the space group of the framework, *C*2/*m*, as described in the Experimental Section. Previously refined framework coordinates of H-TNU-9,[8] along with energy minimized positions of organic SDA molecules, were employed as a starting model in a Rietveld refinement of as-made TNU-9 against high-resolution powder XRD data. Molecular simulation predicted a maximum filling of eight 1,4-MPB molecules per unit cell. Assuming static disorder of the SDA molecules over all the symmetrically equivalent positions in space group *C*2/*m*, this corresponds to a fractional occupancy of 0.25 for each of the four different sites. Fourier difference maps revealed two areas of residual electron density within pore regions not occupied by the organic molecules. These may represent adsorbed water molecules and were introduced to the refinement as O atoms. While their occupancies refined to greater than 1 (and were therefore capped at one), their inclusion improved the *R* values by approximately 1.5%. No further meaningful electron density peaks were identified. The refined unit cell parameters were $a = 28.2377(4)$ Å, $b = 20.0782(3)$ Å, $c = 19.4532(4)$ Å, $\beta = 92.593(1)°$, and R_{wp} and R_p values of 13.47% and 9.55% were achieved. To probe the plausibility of the modeled SDA positions, their fractional occupancies were set to zero and allowed to refine (with all atomic fractional occupancies constrained to be equal). After only a few cycles, fractional occupancies had refined to 0.258(1). Attempts to allow the fractional occupancy of each organic SDA molecule to refine independently resulted in values of 0.263(2), 0.273(2), 0.266(2), and 0.227(3) for molecules 1, 2, 3, and 4, respectively. Consequently, fractional occupancies for molecules 1, 2, and 3 were capped at 0.25, while the occupancy of molecule 4 was permitted to refine. A final occupancy of 0.230(3) was obtained for this molecule, with a global isotropic displacement parameter of 0.009(9) for all molecules. The R_{wp} and R_p values obtained were 13.35% and 9.50%, respectively. Refinement of SDA molecule occupancies after the inclusion of all H atoms to the refinement yielded values of 0.246(2), 0.232(2), 0.256(3), and 0.170(3) for molecules 1, 2, 3, and 4, respectively. The occupancy of molecule 3 was therefore capped at 0.25, and with a globally refined isotropic displacement parameter of 0.04(1) for all organic SDA molecule atoms, R_{wp} and R_p values of 13.13% and 9.30% were achieved, respectively. The refined atomic parameters and selected bond lengths and angles for as-made TNU-9 with energy minimized SDA and water molecule locations are given in Supporting Information Table 1S.

All organic SDA molecule atom coordinates were then permitted to refine without including H atoms. In order to maintain a sensible model, C−C and N−C bond distances were constrained to 1.54 Å ($\sigma = 0.01$ Å) and 1.47 Å ($\sigma = 0.01$ Å), respectively, while the tetrahedral geometry was maintained by constraining nonbonding $(C-C)_N$, $(C-C)_C$, and $(C-N)_C$ distances to 2.40 Å ($\sigma = 0.02$ Å), 2.51 Å ($\sigma = 0.02$ Å), and 2.46 Å ($\sigma = 0.02$ Å), respectively. Once again the occupancies of all SDA molecules were capped at 0.25, and their isotropic displacement parameters were also fixed at their previously refined value of 0.015. "Water" molecule 2 was removed since it was found to encroach upon SDA molecule 2, and the

occupancy and isotropic displacement parameter of "water" molecule 1 were fixed at 1 and 0.025, respectively. SDA molecules 1 and 2 refined sensibly, but molecules 3 and 4 moved to positions that overlapped in space, even when disorder effects were taken into account. Since molecules 3 and 4 continued to overlap, the occupancy of molecule 3 was reduced to 0.125 (at which occupancy an ordering arrangement could be envisaged) and Fourier difference maps were employed in an attempt to locate possible water molecules/Na^+ ions in the unoccupied space. However, only one plausible position was identified within this region and was introduced to the refinement as an oxygen atom, and refinement of the complete model proved difficult with molecules 3 and 4 becoming distorted. The positions of molecules 3 and 4 were subsequently reset to and fixed at those obtained from energy minimization calculations, with occupancies of 0.25. With SDA molecules 3 and 4 fixed at their energy minimized positions, framework coordinates and isotropic displacement parameters refining and atomic coordinates of organic SDA molecules 1 and 2 and 'Na^+' refining, final R_{wp}, R_p, and χ^2 values of 13.60%, 9.60%, and 7.90 were achieved, respectively. The final unit cell parameters obtained were $a = 28.2387(6)$ Å, $b = 20.0792(5)$ Å, $c = 19.4540(6)$ Å, $\beta = 92.593(2)°$. The final atomic positions and isotropic displacement parameters are listed in Table 3 with the final Rietveld plot displayed in Figure 7. Si−O bond lengths refined to values between 1.58(1) and 1.62(1) Å, while O−Si−O and Si−O−Si angles were in the ranges 103(1)°−114(1)° and 132-(3)°−179(2)°, respectively (Supporting Information Table 2S), which are consistent with such values in zeolitic materials. The refined positions of SDA molecules 1 and 2 are shown in Figure 8. Comparison with Figure 5 reveals that these molecules have refined to positions that are very similar to those found from energy minimization calculations.

Elemental analysis reveals that the total organic content in the standard TNU-9 sample, synthesized under rotation (100 rpm) at 433 K for 14 days, is 11.9 wt % (C, 8.69; H, 1.71; N, 1.49), giving a C/N ratio of 6.80 that is slightly lower than the ratio (7) of 1,4-MPB. Assuming that all the 1,4-MPB cations are occluded intact in TNU-9, the overall combination of elemental and thermal analyses yielded a unit cell composition of $|Na_{1.5}(1,4\text{-MPB})_{3.9}(1,4\text{-MPB(OH)}_2)_{3.2}(H_2O)_{28.3}|\ [Al_{9.3}Si_{182.7}O_{384}]$ where OH has been introduced to compensate for the imbalance between the amount of Al and the sum of organic and alkali cations. This suggests that there are, at maximum, seven organic SDA molecules per unit cell, and ^{13}C MAS NMR studies (see below) suggest that as well as the starting organic SDA there could be fragments of other molecules present. Therefore, from the modeling studies, we speculate that, while three (positions **1**, **2** and **4**) of the four suggested positions are likely to be full of the initial SDA molecule, position 3 could contain other organic species (probably SDA decomposition products) and water molecules. This would be expected to give a very similar diffraction pattern to that calculated in the refinement.

3.3. Characterization. The powder XRD pattern of H-TNU-9 agrees well with that of as-made TNU-9, except that the relative intensities of lower angle peaks increase somewhat and there are some small changes in the peak positions (Supporting Information Figure 2S). We also found that all the characteristic X-ray peaks of H-TNU-9 remain intact even after the nitric acid treatment at 363 K for 18 h followed by steaming with 100% water vapor at 1123 K for 3 days, revealing its extremely high hydrothermal stability that is of great practical importance for catalytic applications. From Ar adsorption experiments on H-TNU-9, the type I isotherm indicates a BET surface area of 490 $m^2 \cdot g^{-1}$ and a microporous pore volume of 0.155 $cm^3 \cdot g^{-1}$, which can be expected for multidimensional medium-pore zeolites. The SEM image shows that TNU-9 appears typically as rodlike crystals that are ca. 1.0 μm in length and 0.3 μm in diameter (Supporting Information Figure 3S). The TGA/DTA experiments reveal that there is a small weight loss (1.8 wt %) between room temperature and 523 K, as well as a large weight loss (∼13 wt %) between 523 and 973 K accompanied by two exotherms around 770 and 870 K, as also shown in Supporting Information Figure 3S.

As described above, on the other hand, an unusual feature of the synthesis of TNU-9 is that this zeolite is readily formed at the expense of MCM-22(P) in the crystallization medium. To gain some more insight into the microscopic process involved in such an in situ transformation, the products obtained after heating the 1,4-MPB-containing synthesis mixture with the optimized oxide composition ($SiO_2/Al_2O_3 = 60$ and $NaOH/SiO_2 = 0.73$) for TNU-9 formation under rotation (100 rpm) at 433 K for different periods (5−10 days) of crystallization were studied ex situ by using SEM and ^{27}Al MAS and $^1H-^{13}C$ CP MAS NMR. As shown in Figure 9, the product obtained after 5 days of heating, i.e., MCM-22(P), exhibits two ^{27}Al resonances around 56 and 50 ppm, typical of tetrahedral Al species, and consists of heavily overlapped platelike crystals that are less than 0.1 μm in thickness. These data are in good agreement with those reported previously.[9,18] When the crystallization time is increased to 7 days, a notable decrease in the relative intensity of the low-field ^{27}Al resonance was observed. Clearly, this is a result of the solution-mediated transformation of MCM-22(P) into TNU-9, which can be further supported by the existence of two different crystal morphologies in the SEM image of the product obtained after 7 days of heating. Therefore, the transformation can be simply considered as a matter of dissolution of the less stable MCM-22(P) and separate crystallization of the more stable TNU-9, since the intermediate crystallization product is a physical mixture of these two phases.

Figure 10 shows the $^1H-^{13}C$ CP MAS NMR spectra of the three products obtained after different periods (5−10 days) of crystallization, together with the liquid ^{13}C NMR spectra of 1,4-DBB, 1-MP, and 1,4-MPB dibromide. The $^1H-^{13}C$ CP MAS NMR spectrum of MCM-22(P), obtained after heating for 5 days, exhibits signs of three components in the region 45−55 ppm where only one resonance of the methyl carbons in the *N*-methylpyrrolidinium rings of 1,4-MPB should be otherwise observed. This is also the case for the products obtained after 7 and 10 days that are a physical mixture of MCM-22(P) and TNU-9 with an approximately 30:70 ratio and a highly crystalline TNU-9, respectively (Figure 3). Unlike the other two resonances in the region 45−55 ppm, however, the ^{13}C resonance around 53 ppm was found to show an increase in its relative intensity with longer heating times, suggesting that this resonance is not attributable to the 1,4-MPB in each product.

(18) (a) Hunger, M.; Ernst, S.; Weitkamp, J. *Zeolites* **1995**, *15*, 188. (b) Corma, A.; Corell, C.; Fornes, V.; Kolodziejski, W.; Perez-Pariente, J. *Zeolites* **1995**, *15*, 576. (c) Lawton, S. L.; Fung, A. S.; Kennedy, G. J.; Alemany, L. B.; Chang, C. D.; Hatzikos, G. H.; Lissy, D. N.; Rubin, M. K.; Timken, H. K. C.; Steuernagel, S.; Woessner, D. E. *J. Phys. Chem.* **1996**, *100*, 3788.

Table 3. Final Atomic Coordinates and Displacement and Population Parameters for As-Made TNU-9 in *C*2/*m* Symmetry with Standard Deviations in Parentheses

atom	*x*	*y*	*z*	occupancy	U_{iso}, Å^2	multiplicity
Si1	0.1012(7)	0.1880(10)	0.7071(9)	1	0.0130(17)	8
Si2	0.0039(7)	0.3105(11)	0.1464(10)	1	0.0130(17)	8
Si3	0.1529(7)	0.1852(10)	0.1684(10)	1	0.0130(17)	8
Si4	0.0897(7)	0.1176(11)	0.9306(10)	1	0.0130(17)	8
Si5	0.1062(6)	0.3091(10)	0.0855(9)	1	0.0130(17)	8
Si6	0.0049(7)	0.0770(7)	0.1476(11)	1	0.0130(17)	8
Si7	0.1043(7)	0.4274(9)	0.7122(11)	1	0.0130(17)	8
Si8	0.1512(7)	0.4237(8)	0.1724(10)	1	0.0130(17)	8
Si9	0.1014(7)	0.0776(7)	0.0871(10)	1	0.0130(17)	8
Si10	0.2532(7)	0.3797(11)	0.2287(10)	1	0.0130(17)	8
Si11	0.1463(7)	0.0766(7)	0.8041(11)	1	0.0130(17)	8
Si12	0.1661(7)	0.3815(11)	0.4396(10)	1	0.0130(17)	8
Si13	0.1010(7)	0.3772(10)	0.3059(10)	1	0.0130(17)	8
Si14	0.2370(7)	0.0745(8)	0.6148(11)	1	0.0130(17)	8
Si15	0.0006(7)	0.4235(8)	0.2557(12)	1	0.0130(17)	8
Si16	1.0017(7)	0.1893(10)	0.2546(10)	1	0.0130(17)	8
Si17	0.2375(7)	0.3113(11)	0.6219(10)	1	0.0130(17)	8
Si18	0.1420(6)	0.3091(10)	0.7988(9)	1	0.0130(17)	8
Si19	0.1640(7)	0.2210(10)	0.4341(10)	1	0.0130(17)	8
Si20	0.1031(7)	0.2168(10)	0.3047(10)	1	0.0130(17)	8
Si21	0.1681(8)	0.4252(8)	0.5874(11)	1	0.0130(17)	8
Si22	0.0857(7)	0.2771(10)	0.9313(10)	1	0.0130(17)	8
Si23	0.1662(7)	0.1892(11)	0.5838(10)	1	0.0130(17)	8
Si24	0.2524(7)	0.2198(11)	0.2242(10)	1	0.0130(17)	8
O1	0.0402(9)	0.0869(17)	0.9038(17)	1	0.0135(30)	8
O2	0.0850(12)	0.1972(10)	0.9326(19)	1	0.0135(30)	8
O3	0.1283(11)	0.0949(19)	0.8783(13)	1	0.0135(30)	8
O4	0.1035(11)	0.0911(19)	0.0064(10)	1	0.0135(30)	8
O5	0.1225(9)	0.1883(20)	0.6327(12)	1	0.0135(30)	8
O6	0.1220(13)	0.2511(15)	0.7490(18)	1	0.0135(30)	8
O7	0.1184(13)	0.1211(14)	0.7466(17)	1	0.0135(30)	8
O8	0.0446(6)	0.1941(20)	0.7005(14)	1	0.0135(30)	8
O9	0.0508(8)	0.1013(16)	0.1102(18)	1	0.0135(30)	8
O10	0.1063(17)	0	0.1043(24)	1	0.0135(30)	4
O11	0.1426(9)	0.1159(12)	0.1294(16)	1	0.0135(30)	8
O12	0.2013(7)	0.0920(18)	0.8058(18)	1	0.0135(30)	8
O13	0.1367(17)	0	0.7887(25)	1	0.0135(30)	4
O14	0.1203(11)	0.3013(19)	0.8731(12)	1	0.0135(30)	8
O15	0.1051(10)	0.3049(18)	0.0039(9)	1	0.0135(30)	8
O16	0.0346(8)	0.3068(18)	0.9160(13)	1	0.0135(30)	8
O17	0.2091(7)	0.1929(18)	0.1769(15)	1	0.0135(30)	8
O18	0.3013(6)	0.1932(19)	0.1958(17)	1	0.0135(30)	8
O19	0.2457(12)	0.1901(18)	0.2990(10)	1	0.0135(30)	8
O20	0.2533(12)	0.2998(10)	0.2265(19)	1	0.0135(30)	8
O21	0.0527(7)	0.3120(21)	0.1086(16)	1	0.0135(30)	8
O22	1.0014(14)	0.2477(15)	0.1977(16)	1	0.0135(30)	8
O23	−0.0027(13)	0.3783(14)	0.1879(15)	1	0.0135(30)	8
O24	0.1321(13)	0.2449(14)	0.1205(18)	1	0.0135(30)	8
O25	0.1305(11)	0.1846(16)	0.2426(12)	1	0.0135(30)	8
O26	0.1312(12)	0.3774(13)	0.1110(15)	1	0.0135(30)	8
O27	0.0100(17)	0	0.1671(23)	1	0.0135(30)	4
O28	0.9988(13)	0.1189(12)	0.2161(14)	1	0.0135(30)	8
O29	0.1280(11)	0.4129(22)	0.6409(13)	1	0.0135(30)	8
O30	0.0483(7)	0.4171(23)	0.7061(17)	1	0.0135(30)	8
O31	0.1270(12)	0.3806(11)	0.7703(15)	1	0.0135(30)	8
O32	0.1192(19)	0.5	0.7369(26)	1	0.0135(30)	4
O33	0.1249(12)	0.4094(17)	0.2414(13)	1	0.0135(30)	8
O34	0.1450(16)	0.5	0.1500(22)	1	0.0135(30)	4
O35	0.2062(7)	0.4072(19)	0.1885(17)	1	0.0135(30)	8
O36	0.2521(13)	0.4056(19)	0.3066(11)	1	0.0135(30)	8
O37	0.1683(12)	0.3010(10)	0.4401(19)	1	0.0135(30)	8
O38	0.2166(8)	0.4131(18)	0.4262(17)	1	0.0135(30)	8
O39	0.1495(10)	0.4095(19)	0.5108(10)	1	0.0135(30)	8
O40	0.1275(11)	0.3989(15)	0.3777(13)	1	0.0135(30)	8
O41	0.0466(7)	0.4023(19)	0.3028(16)	1	0.0135(30)	8
O42	0.1042(13)	0.2970(9)	0.2987(18)	1	0.0135(30)	8
O43	0.1933(10)	0.1192(13)	0.5873(19)	1	0.0135(30)	8
O44	0.2190(14)	0	0.6082(27)	1	0.0135(30)	4
O45	0.0061(19)	0.5	0.2323(25)	1	0.0135(30)	4
O46	0.0493(7)	0.1913(19)	0.3026(15)	1	0.0135(30)	8
O47	0.2135(9)	0.3820(12)	0.6085(19)	1	0.0135(30)	8
O48	0.2845(8)	0.3084(18)	0.5787(16)	1	0.0135(30)	8
O49	0.2010(12)	0.2510(14)	0.6037(21)	1	0.0135(30)	8

Table 3 (Continued)

atom	*x*	*y*	*z*	occupancy	U_{iso}, Å^2	multiplicity
O50	0.1457(10)	0.1948(18)	0.5060(9)	1	0.0135(30)	8
O51	0.1277(10)	0.1944(16)	0.3758(11)	1	0.0135(30)	8
O52	0.1857(17)	0.5	0.5928(28)	1	0.0135(30)	4
1N1	0.505(9)	0.121(4)	0.491(14)	0.25	0.0147	8
1C1	0.481(13)	0.170(9)	0.445(17)	0.25	0.0147	8
1C2	0.491(21)	0.240(6)	0.475(24)	0.25	0.0147	8
1C3	0.510(19)	0.228(10)	0.550(23)	0.25	0.0147	8
1C4	0.507(13)	0.151(12)	0.560(14)	0.25	0.0147	8
1C5	0.481(9)	0.056(6)	0.488(19)	0.25	0.0147	8
1C6	0.507(13)	0.0000	0.527(15)	0.5	0.0147	4
1C7	0.514(13)	−0.064(5)	0.485(20)	0.25	0.0147	8
1C8	0.480(8)	−0.120(5)	0.501(19)	0.25	0.0147	8
1C9	0.510(12)	−0.200(14)	0.584(11)	0.25	0.0147	8
1N2	0.497(7)	−0.187(5)	0.511(11)	0.25	0.0147	8
1C10	0.460(8)	−0.236(6)	0.490(16)	0.25	0.0147	8
1C11	0.485(11)	−0.303(5)	0.479(16)	0.25	0.0147	8
1C12	0.538(11)	−0.285(9)	0.475(17)	0.25	0.0147	8
1C13	0.539(9)	−0.207(9)	0.473(16)	0.25	0.0147	8
1C14	0.554(9)	0.112(13)	0.470(18)	0.25	0.0147	8
2N1	0.576(4)	0.5000	0.486(6)	0.5	0.0147	4
2C1	0.625(5)	0.5000	0.516(7)	0.5	0.0147	4
2C2	0.658(5)	0.503(21)	0.454(12)	0.25	0.0147	8
2C3	0.626(9)	0.485(17)	0.390(8)	0.25	0.0147	8
2C4	0.578(7)	0.466(8)	0.419(8)	0.25	0.0147	8
2C5	0.542(6)	0.471(7)	0.532(12)	0.25	0.0147	8
2C6	0.501(7)	0.518(9)	0.548(15)	0.25	0.0147	8
2C7	0.464(6)	0.487(17)	0.594(13)	0.25	0.0147	8
2C8	0.417(6)	0.527(13)	0.591(13)	0.25	0.0147	8
2C9	0.389(9)	0.423(12)	0.635(16)	0.25	0.0147	8
2N2	0.380(4)	0.495(14)	0.628(6)	0.25	0.0147	8
2C10	0.333(5)	0.504(25)	0.593(7)	0.25	0.0147	8
2C11	0.296(4)	0.499(32)	0.650(11)	0.25	0.0147	8
2C12	0.325(8)	0.508(23)	0.719(8)	0.25	0.0147	8
2C13	0.376(7)	0.523(15)	0.698(8)	0.25	0.0147	8
2C14	0.563(5)	0.5698(23)	0.471(9)	0.25	0.0147	8
3N1	0.2967	0.9941	0.0523	0.25	0.0147	8
3C1	0.2963	0.9339	0.0985	0.25	0.0147	8
3C2	0.2668	0.9526	0.1600	0.25	0.0147	8
3C3	0.2788	1.0260	0.1703	0.25	0.0147	8
3C4	0.2813	1.0515	0.0966	0.25	0.0147	8
3C5	0.3452	1.0055	0.0226	0.25	0.0147	8
3C6	0.3897	1.0201	0.0705	0.25	0.0147	8
3C7	0.4300	0.9678	0.0683	0.25	0.0147	8
3C8	0.4580	0.9633	0.0009	0.25	0.0147	8
3C9	0.5020	1.0689	0.0173	0.25	0.0147	8
3N2	0.5061	0.9975	−0.0029	0.25	0.0147	8
3C10	0.5449	0.9637	0.0385	0.25	0.0147	8
3C11	0.5915	0.979	0.0027	0.25	0.0147	8
3C12	0.5777	0.999	−0.0709	0.25	0.0147	8
3C13	0.5236	0.9932	−0.0736	0.25	0.0147	8
3C14	0.2614	0.9842	−0.007	0.25	0.0147	8
4N1	0.2405	0.5805	0.9807	0.25	0.0147	8
4C1	0.1987	0.6247	0.9915	0.25	0.0147	8
4C2	0.2167	0.6970	0.9915	0.25	0.0147	8
4C3	0.2644	0.6904	1.0298	0.25	0.0147	8
4C4	0.2822	0.6223	1.0061	0.25	0.0147	8
4C5	0.2355	0.5162	1.0213	0.25	0.0147	8
4C6	0.2758	0.4636	1.0216	0.25	0.0147	8
4C7	0.2755	0.4132	0.9619	0.25	0.0147	8
4C8	0.2376	0.3575	0.9544	0.25	0.0147	8
4C9	0.2312	0.31	1.0674	0.25	0.0147	8
4N2	0.2416	0.2932	0.9959	0.25	0.0147	8
4C10	0.2068	0.2411	0.9695	0.25	0.0147	8
4C11	0.2303	0.1732	0.9775	0.25	0.0147	8
4C12	0.2812	0.1896	0.9627	0.25	0.0147	8
4C13	0.2891	0.2587	0.9944	0.25	0.0147	8
4C14	0.2434	0.5654	0.9053	0.25	0.0147	8
Na1	0.456(4)	0.5	0.392(7)	0.5	0.025	4

Comparison with the liquid ^{13}C NMR spectra of organic precursors led us to interpret it as the methyl carbon in 1-MP. As marked with an arrow in Figure 10, furthermore, the ^{1}H−^{13}C CP MAS NMR spectrum of the product obtained after 10 days shows a weak but non-negligible resonance around 30 ppm which is assignable to methylamine (MA).[19] Therefore, it is most

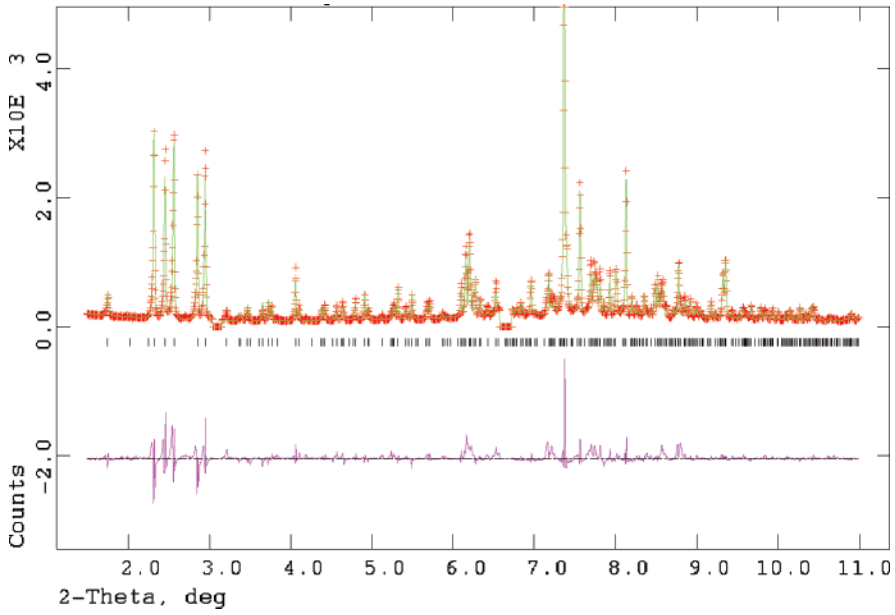

Figure 7. Rietveld plot from 1.5° to 11.0° 2θ for as-made TNU-9 after permitting atomic coordinates of organic SDA molecules 1 and 2 to refine individually: observed data (crosses), calculated profile (solid line), and difference (lower trace). The tick marks represent the positions of allowed reflections.

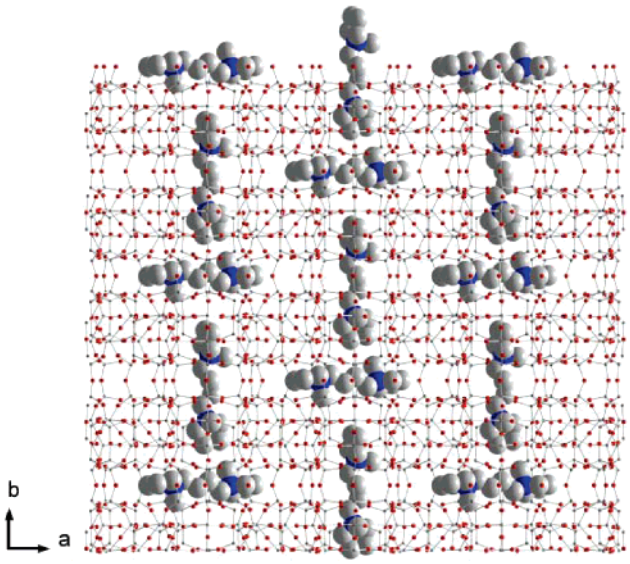

Figure 8. Refined locations of organic SDA molecules 1 and 2 within intersheet region I in the TNU-9 framework.

likely that a small fraction of the 1,4-MPB molecules has decomposed to probably give smaller amines under the synthesis conditions, while most of them are occluded intact in TNU-9. This can be rationalized by suggesting that 1,4-MPB may have limited stability under the rather basic conditions (pH ~11.5) for TNU-9 formation. Among the other seven zeolitic phases that can also be prepared with 1,4-MPB, in fact, TNU-10 and mordenite obtained using gels with $NaOH/SiO_2 > 0.73$ and hence with higher pH values exhibited additional ^{13}C resonances around 53 ppm and/or 30 ppm in their $^1H-^{13}C$ CP MAS NMR spectra (Supporting Information Figure 4S).

The total organic content in MCM-22(P) obtained after heating for 5 days was determined to be 16.4 wt % (C, 11.71; H, 2.75; N, 1.94). While this value is considerably high compared to that (11.9 wt %) in TNU-9, it gives a C/N ratio (7.04) that is very close to the ratio (7) of 1,4-MPB. As shown in Figure 10, furthermore, the ^{13}C resonances other than those from 1,4-MPB are hardly visible in the $^1H-^{13}C$ CP MAS NMR spectrum of this product. Thus, the partial degradation of organic

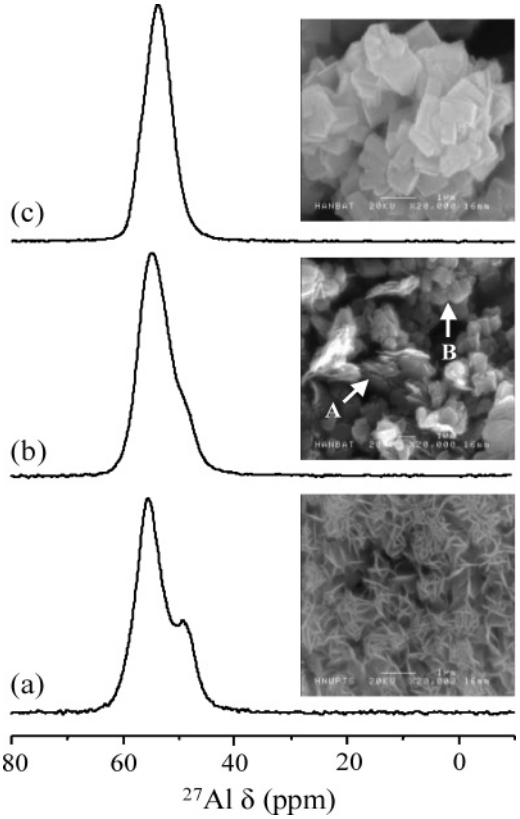

Figure 9. ^{27}Al MAS NMR spectra and SEM images of the products obtained after heating the 1,4-MPB-containing synthesis mixture with the optimized gel composition ($SiO_2/Al_2O_3 = 60$ and $NaOH/SiO_2 = 0.73$) for TNU-9 formation under rotation (100 rpm) at 433 K for (a) 5, (b) 7, and (c) 10 days. Labels A and B in the SEM image indicate MCM-22(P) and TNU-9 crystallites, respectively.

(19) Breitmaier; Voelter, W. *^{13}C NMR Spectroscopy*, 2nd ed.; Verlag Chemie: Weinheim, 1978; p 178.

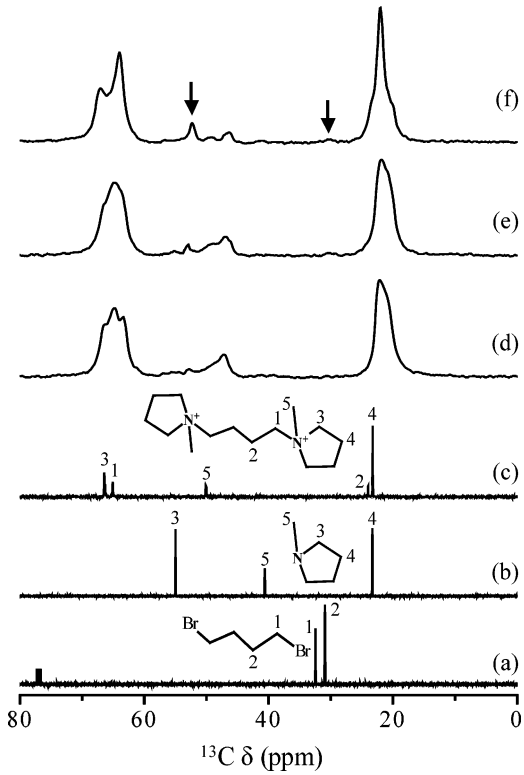

Figure 10. ^{13}C NMR spectra of (a) 1,4-DBB in $CDCl_3$ solution, (b) 1-MP in D_2O solution, and (c) 1,4-MPB dibromide in D_2O solution, showing the assignment of each resonance, and ^{1}H−^{13}C CP MAS NMR spectra of the products obtained after heating the 1,4-MPB-containing synthesis mixture with the optimized gel composition for TNU-9 formation under rotation (100 rpm) at 433 K for (d) 5, (c) 7, and (d) 10 days. The arrows denote resonances that are not attributable to 1,4-MPB.

SDA molecules at the crystallization stage of MCM-22(P) appears to be negligible. Because the TNU-9 structure has short bridging 10-ring channels between the channels B, on the other hand, one can wonder whether the 1,4-MPB cation having relatively large 1-methylpyrrolidinium rings is positioned within such channels, without experiencing severe geometric constraints and van der Waals interactions with the zeolite framework. Although hydrated Na^+ ions, counterbalancing AlO_4^- units in the framework, are likely to serve as a good pore filler in such short channels, we believe that the stabilization of the three-dimensional TNU-9 channel system could be better achieved by a cooperative structure-directing effect of 1,4-MPB and its smaller decomposition products, most likely 1-MP and MA, as supported by the ^{1}H−^{13}C CP MAS NMR results in Figure 10, and also proposed in the synthesis of ITQ-1, the pure-silica version of MCM-22, in which the *N*,*N*,*N*,-trimethyl-1-adamantammonium ion was used as an organic SDA.[20] This would also explain why the presence of excess 1-MP in the synthesis mixture in which 1,4-DBB and 1-MP, instead of 1,4-MPB, are used as organic SDAs accelerates the crystallization of TNU-9 (Table 1). Because the molecular modeling results in Figure 5 and Table 2 suggest that the 1,4-MPB molecule is a close fit for positions **1**, **2**, and **4**, with position **3** in the short bridging 10-ring channel less favored, in particular, it is most likely that while three of the four suggested positions in TNU-9 may be full of the initial SDA, the fourth (i.e., position **3**) could contain 1-MP and/or MA. This appears to be a sensible explanation since there are many possible zeolite structures in which the organic SDA positions are different enough to be better filled by two or more different species.

The ^{1}H−^{13}C CP MAS NMR spectrum of TNU-9 obtained using a mixture of 1,4-DBB and 1-MP with a molar ratio of 1:2, instead of 1,4-MPB, under rotation (100 rpm) at 433 K for 14 days can be found in Supporting Information Figure 5S. While this spectrum clearly shows the in situ formation of 1,4-MPB in the synthesis conditions, which must be subsequently responsible for the crystallization of TNU-9, there are two additional weak ^{13}C resonances around 53 and 30 ppm that are attributable to 1-MP and MA, respectively. It is interesting to note here that we were also able to obtain IM-5, another new medium-pore zeolite,[6a,16,17] by directly introducing 1,5-dibromopentane and 1-MP with a molar ratio of 1:2, instead of 1,5-MPP known as an SDA yielding this zeolite, in the synthesis mixture. Since the ^{1}H−^{13}C CP MAS NMR spectrum (Supporting Information Figure 6S) of IM-5 prepared via the above way evidences the presence of 1,5-MPP in its pores, the in situ formation of organic SDAs, especially of diquaternary alkylammonium ions, during the synthesis of a particular structure type of zeolites appears to be more common than once expected.[21]

Figure 11 shows the ^{27}Al and ^{29}Si MAS NMR spectra of the as-made and proton forms of TNU-9. Unlike the spectrum of as-made TNU-9 characterized by only one ^{27}Al resonance at 53.6 ppm, that of H-TNU-9 gives an additional ^{27}Al resonance around 0 ppm. This reveals that a portion of framework Al atoms has been extracted from the TNU-9 framework during the calcination and exchange steps, which can be further supported by comparing the ^{29}Si MAS NMR spectrum of as-made TNU-9 with that of H-TNU-9. Figure 11 also shows the ^{29}Si MAS NMR spectrum of dealuminated TNU-9 prepared via the initial nitric acid treatment at 363 K and the subsequent steaming at 1123 K. N_2 adsorption of this sample gives a BET surface area of 405 $m^2 \cdot g^{-1}$ that is 80% of the value (506 $m^2 \cdot g^{-1}$) of the parent H-TNU-9 sample, revealing that the overall structural integrity of TNU-9 remains intact even after dealumination under such severe conditions, as also evidenced by powder XRD experiments. According to the structure of TNU-9, on the other hand, a maximum of 24 ^{29}Si resonances with equal populations is expected for the basically Al-free framework. Although the dealumination conditions employed here were so severe, however, deconvolution of the ^{29}Si MAS NMR spectrum of the dealuminated sample indicates the presence of only nine $Si(OSi)_4$ sites with a relative intensity ratio of approximately 2:2:4:3:5:1:1:1:2 from −108.7 to −115.8 ppm. The fact that their full widths at half-maximum are 50−90 Hz at a ^{29}Si frequency of 99.352 MHz indicates that the amount of framework Al atoms in dealuminated TNU-9 is still large enough to cause heavy line broadening and hence severe overlapping of ranges for different $Si(OSi)_4$ species. Due to the narrow chemical shift range (∼7 ppm) observed for dealuminated TNU-9, in addition, the accurate assignment of its individual ^{29}Si reso-

(20) Camblor, M. A.; Corma, A.; Diaz-Cabanas, M.-J.; Baerlocher, Ch. *J. Phys. Chem. B* **1998**, *102*, 44.

(21) (a) Rao, G. N.; Joshi, P. N.; Kotasthane, A. N.; Ratnasamy, P. *Zeolites* **1989**, *9*, 483. (b) Bats, N.; Rouleau, L.; Paillaud, J.-L.; Caullet, P.; Mathieu, Y.; Lacombe, S. In *Proceedings of the 14th International Zeolite Conference*; van Steen, E.; Callanan, L. H.; Claeys, M., Eds.; Document Transformation Technologies: Cape Town, 2004; p 283.

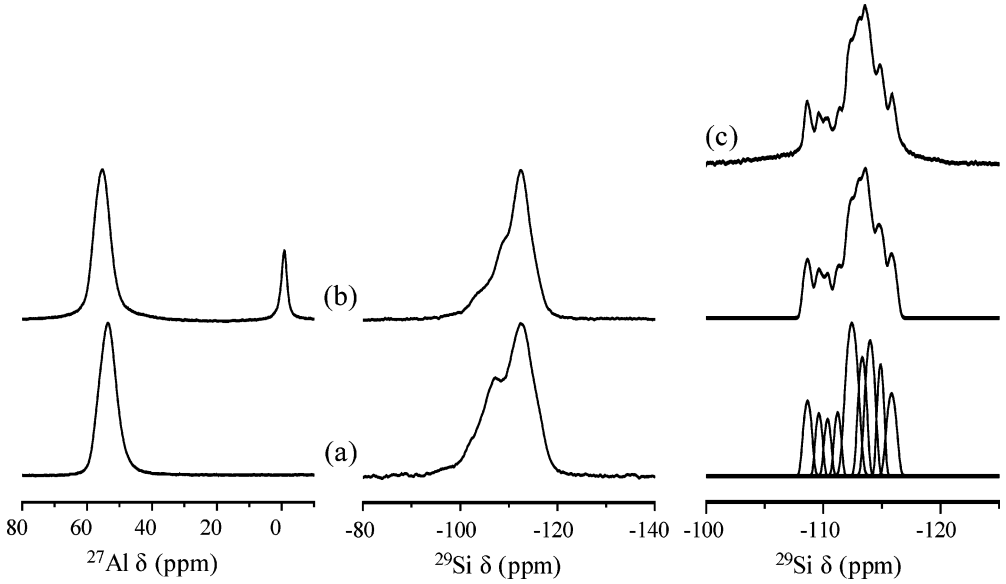

Figure 11. ^{27}Al (left) and ^{29}Si (middle) MAS NMR spectra of (a) as-made TNU-9, (b) H-TNU-9, and (c) deconvoluted components and simulated and experimental patterns (bottom to top) of ^{29}Si (right) MAS NMR spectrum of dealuminated TNU-9.

nances to distinct T-sites should be awaited until a more siliceous phase is prepared.

The pore size distribution (PSD) curves of H-TNU-9 and H-ZSM-5 calculated from their Ar adsorption isotherms using the Horvath−Kawazoe formalism[22] are given in Supporting Information Figure 7S. The PSD curve for H-ZSM-5 with an intersecting 10-ring pore system between the straight (5.3 × 5.6 Å) and the sinusoidal (5.1 × 5.5 Å) channels is characterized by one sharp maximum around 5.2 Å. Although the general feature of this curve is similar to that of the curve of H-TNU-9, however, a much broader maximum around 5.3 Å was observed for the latter curve. This can be rationalized by considering that the difference (0.5 vs 0.1 Å) in the longest diameter of 10-ring channels is fairly larger in TNU-9 than in ZSM-5. The Ar adsorption isotherms of these two zeolites are also shown in Supporting Information Figure 7S. Although the pores in both materials start to fill up at a relative pressure of $P/P_o \approx 5 \times 10^{-6}$, H-TNU-9 gives a second inflection point in the vicinity of $P/P_o = 5 \times 10^{-3}$, unlike H-ZSM-5. This is probably due to the filling of its large cavities that are circumscribed by 12-ring openings but are accessible only through 10-ring openings (Figure 6), which can be correlated to the presence of a very broad maximum around 7.2 Å in the PSD curve.

Figure 12 shows the IR spectra of H-TNU-9 before and after pyridine adsorption followed by desorption at different temperatures. Five different types of hydroxyl groups can be observed from the IR spectrum of dehydrated H-TNU-9. Three well-resolved bands appearing at 3737, 3670, and 3614 cm^{-1} are commonly assigned to silanol groups on the external surface of H-TNU-9 crystallites, hydroxyl groups bonded to extraframework Al, and acidic bridging hydroxyl groups, respectively.[23] While a very weak band around 3781 cm^{-1} is attributable to the terminal hydroxyl groups bonded to extraframework AlOOH, the broad band in the region 3400−3600 cm^{-1} can be assigned to hydrogen-bonded Si−(OH)$^+$−Al bridges with SiOH groups

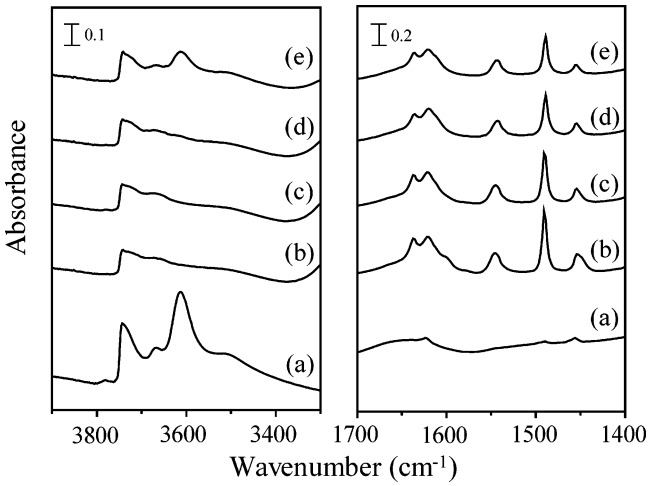

Figure 12. IR spectra of H-TNU-9 in the hydroxyl stretching (left) and C−C stretching (right) regions (a) before and after pyridine adsorption followed by desorption at (b) 473, (c) 573, (d) 673, and (c) 773 K for 1 h.

or hydroxyl groups in framework-defect sites.[24] After pyridine adsorption the band at 3614 cm^{-1} disappears completely and two bands associated with the pyridinium ion adsorbed at Brönsted acid sites and pyridine coordinated to Lewis acid sites appear around 1545 and 1455 cm^{-1}, respectively. With the increase of desorption temperature the intensity of the two bands around 1545 and 1455 cm^{-1} is reduced, but a considerable fraction of both the pyridinium ion and pyridine still remains adsorbed at 773 K, indicating the presence of very strong acid sites in H-TNU-9.

3.4. Catalysis. The projection of TNU-9 down the *b*-axis (Figure 1) is very similar to that of ZSM-5, one of the most widely studied and industrially important zeolites, but the pore connectivity in the third direction is much more complex. Therefore, it is of great practical importance to investigate the

(22) Horvarth, G.; Kawazoe, K. J. *J. Chem. Eng. Jpn.* **1983**, *16*, 470.
(23) Jentys, A.; Lercher, J. A. *Stud. Surf. Sci. Catal.* **2001**, *137*, 345.
(24) (a) Kiricsi, I.; Flego, C.; Pazzuconi, G.; Parker, W. O.; Millini, R.; Perego, C.; Bellussi, G. *J. Phys. Chem.* **1994**, *98*, 4627. (b) Jia, C.; Massiani, P.; Barthomeuf, D. *J. Chem. Soc., Faraday Trans.* **1993**, *89*, 3659. (c) Martinez-Triguero, J.; Diaz-Cabanas, M. J.; Camblor, M. A.; Fornes, V.; Maesen, Th. L. M.; Corma, A. *J. Catal*. **1999**, *182*, 463.

Table 4. Conversion and Product Distribution in Toluene Disproportionation over H-TNU-9, H-ZSM-5, H-MCM-22, H-Mordenite, and H-Beta Zeolites[a]

catalyst	H-TNU-9		H-ZSM-5		H-MCM-22		H-ordenite		H-beta	
time on stream, min	0	240	0	240	0	240	0	240	0	240
conversion, mol %	38.1	5.43	2.13	0.63	45.3	1.96	25.8	4.41	6.56	2.13
product yields, mol %										
$<C_6$	0.26	0.03	0.02	0.02	0.08	0.02	0.08	0.03	0.00	0.04
benzene	18.41	2.47	1.25	0.27	21.84	0.88	12.35	2.03	3.09	1.52
ethylbenzene	0.09	0.03	0.02	0.03	0.03	0.03	0.00	0.00	0.00	0.05
p-xylene	4.21	0.76	0.35	0.07	6.27	0.42	3.03	0.64	0.87	0.48
m-xylene	9.16	1.60	0.72	0.14	12.88	0.51	6.81	1.21	1.82	0.96
o-xylene	3.63	0.45	0.27	0.06	4.23	0.10	2.73	0.46	0.79	0.37
C_{9+}	1.14	0.08	0.02	0.02	0.01	0.00	0.76	0.04	0.06	0.09
benzene/xylenes	1.08	0.88	0.93	1.00	0.93	0.85	0.98	0.88	0.89	0.84
fraction in xylenes, %										
p-xylene	24.8	27.1	26.1	25.9	26.8	40.8	24.1	27.7	25.0	26.5
m-xylene	54.9	56.9	53.7	51.9	55.1	49.5	54.2	52.4	52.3	53.1
o-xylene	21.3	16.0	20.2	22.2	18.1	9.7	21.7	19.9	22.7	20.4

[a] Reaction conditions: 573 K, 0.2 g of catalyst, 16.5 kPa of toluene pressure, 7.2 h^{-1} of WHSV.

Table 5. Initial Conversion and Product Distribution in *m*-Xylene Isomerization and Disproportionation over Various Zeolite Catalysts at 623 K and 20.3 kPa *m*-Xylene Pressure

catalyst	H-TNU-9	H-ZSM-5	H-MCM-22	H-mordenite	H-beta	equilibrium
WHSV, min^{-1}	3.0	4.1	2.4	4.7	3.0	
conversion, mol %	22.0	20.6	19.3	18.8	23.2	
product yields, mol %						
isomerization (*i*)	16.50	20.25	18.11	12.33	15.18	
disproportionation (*d*)	5.26	0.31	1.06	6.19	7.86	
i/*d*	3.1	65	17	2.0	1.9	
product distribution,[a] mol %						
$<C_6$	0.14	0.00	0.14	0.01	0.01	
benzene	0.07	0.00	0.00	0.12	0.06	
toluene	3.31	0.20	0.91	3.71	4.79	
p-xylene	12.90	13.83	11.78	6.66	8.37	
o-xylene	3.60	6.42	6.33	5.67	6.81	
1,3,5-trimethylbenzene (TMB)	0.02	0.01	0.03	0.60	0.85	
1,2,4-TMB	1.93	0.10	0.12	1.68	2.00	
1,2,3-TMB	0.00	0.00	0.00	0.20	0.22	
C_{10+}	0.01	0.00	0.00	0.18	0.12	
p-xylene/*o*-xylene	3.6	2.2	1.9	1.2	1.2	1.0
toluene/TMBs	1.7	1.8	6.7	1.5	1.6	
normalized TMB distribution, mol %						
1,3,5-TMB	1.0	9.1	20.0	24.2	27.7	24.0
1,2,4-TMB	99.0	90.9	80.0	67.7	65.1	68.0
1,2,3-TMB	0.0	0.0	0.0	8.1	7.2	8.0
1,2,3-TMB/1,3.5-TMB	0.00	0.00	0.00	0.33	0.26	0.33

[a] *m*-Xylene was not included.

performance of TNU-9 for commercial petrochemical processes that are known to use ZSM-5-type zeolites as shape selective catalysts.[25] For this purpose we have chosen the disproportionation of toluene and the isomerization and disproportionation of *m*-xylene as two test reactions. The characteristics of all five zeolites with different framework structures employed in this study can be found in Supporting Information Table 3S. Because there are no significant differences in the physicochemical properties of these zeolites, e.g., crystallite size and acidity, the catalytic results from the gas-phase transformation of toluene and *m*-xylene could be mainly regarded as a reflex of geometrical constraints imposed by the particular pore structure of each zeolite.

Table 4 lists the initial conversions and product distributions in the disproportionation of toluene over H-TNU-9, H-ZSM-5, H-MCM-22, H-mordenite, and H-beta at 573 K, 7.2 h^{-1} WHSV, and 16.5 kPa toluene in the feed, which were not influenced by coke formation, together with the steady-state data measured after 240 min on stream under the identical reaction conditions. H-TNU-9 exhibits a lower initial toluene conversion (38 vs 45%) than H-MCM-22, which has two independent 10-ring pore systems, one formed by two-dimensional sinusoidal 10-ring (4.1 × 5.1 Å) channels and the other by large cylindrical supercages (7.1 Å in diameter and 18.2 Å in height) that are accessible only through 10-ring (4.0 × 5.5 Å) windows.[1] However, the initial activity of H-TNU-9 is quite high compared to that of large-pore H-mordenite and H-beta, and especially to that of medium-pore H-ZSM-5, which is almost inactive at 573 K. Considering that the intersecting 10-ring pore system of ZSM-5 does not allow the formation of the bulky transition state at this temperature,[26] it appears that the bimolecular toluene disproportionation over H-TNU-9 may occur mainly on the Brönsted acid sites within the large 12-ring cavities rather than within the two main 10-ring channels along the *b*-axis. The

(25) Degnan, T. F. *J. Catal.* **2003**, *216*, 32.

(26) (a) Kaeding, W. W.; Chu, C.; Young, L. B.; Butter, S. A. *J. Catal.* **1981**, *69*, 392. (b) Xiong, Y. S.; Rodewald, P. G.; Chang, C. D. *J. Am. Chem. Soc.* **1995**, *117*, 9427. (c) Wu, P.; Komatsu, T.; Yashima, T. *Microporous Mesoporous Mater.* **1998**, *22*, 343.

toluene conversion as a function of time on stream (TOS) with all zeolites used in this study can be found in Supporting Information Figure 8S. We note that H-TNU-9 deactivates less rapidly than H-MCM-22. Unlike the latter, however, the former showed no noticeable changes in the distribution of xylene isomers during the period of TOS studied here. For example, the fraction (27%) of *p*-xylene measured after 240 min on stream is still in the vicinity of the equilibrium value (24%) at 573 K (Table 4). This suggests that, even after being considerably deactivated, H-TNU-9 behaves like a large-pore zeolite in the toluene disproportionation.

Table 5 gives the catalytic results for the isomerization and disproportionation of *m*-xylene at 623 K and 20.3 kPa *m*-xylene in the feed over the zeolites used in this study. The transformation of *m*-xylene has long been used as a test reaction for proving the effective pore width of zeolites and related microporous materials, especially for distinguishing between 10- and 12-ring pore materials.[27] The initial activities of all the zeolites were found to be generally similar in the isomerization process. However, there are notable differences in the disproportionation activity. Although access to its inner pore space is via 10-ring openings only, H-TNU-9 shows an initial isomerization (*i*) to disproportionation (*d*) ratio much closer to that of large-pore zeolites than that of medium-pore materials, and this cannot be explained on the basis of differences in the acidity of the zeolites studied. It is also not likely to be related to the crystal size, since the H-TNU-9 sample has larger crystals than those of H-ZSM-5 or H-MCM-22 (Supporting Information Table 3S), so the contribution of the external surface to the bimolecular disproportionation is expected to be lower in H-TNU-9. Therefore, we believe that the 12-ring cavities in this medium-pore zeolite may be large enough to allow the formation of three possible bulky transition states required for *m*-xylene disproportionation,[27] whereas the presence of such large cages would give *m*-xylene molecules an increased intracrystalline residence time, leading to more molecular collisions and hence more bimolecular reactions.

It is also remarkable that, among the three trimethylbenzene (TMB) isomers, the initial fraction (99%) of 1,2,4-MTB of H-TNU-9 is much higher than the equilibrium value (68%) at 623 K.[27b] This can be rationalized by considering that the longest pore diameter (6.0 Å) of channel A in TNU-9 is large enough to allow for the egress of 1,2,4-TMB (5.5 × 6.7 Å) while still hindering the easy exit of the other two isomers (5.9 × 6.6 Å). A similar explanation could be given to the low initial disproportionation activity observed for H-MCM-22 with large cylindrical supercages, because none of the three TMB isomers can easily diffuse out through the elliptical 10-ring (4.0 × 5.5 Å) windows of its supercages. When *m*-xylene isomerizes to *p*- and *o*-xylenes, on the other hand, 10-ring pore zeolites are known to give higher *p*/*o* ratios than those of 12-ring pore zeolites, due to differences in the diffusion of both isomers through the narrow channels of the former zeolites, i.e., product shape selectivity.[25−27] As listed in Table 5, H-TNU-9 gives an initial *p*/*o* ratio of 3.6 that is in the expected range for medium-pore zeolites. However, we note that this *p*/*o* ratio is fairly high compared to the value observed for H-ZSM-5 or H-MCM-22, which can be partly attributed to the larger crystal size (Supporting Information Table 3S) of H-TNU-9, giving the zeolite more product shape selectivity.

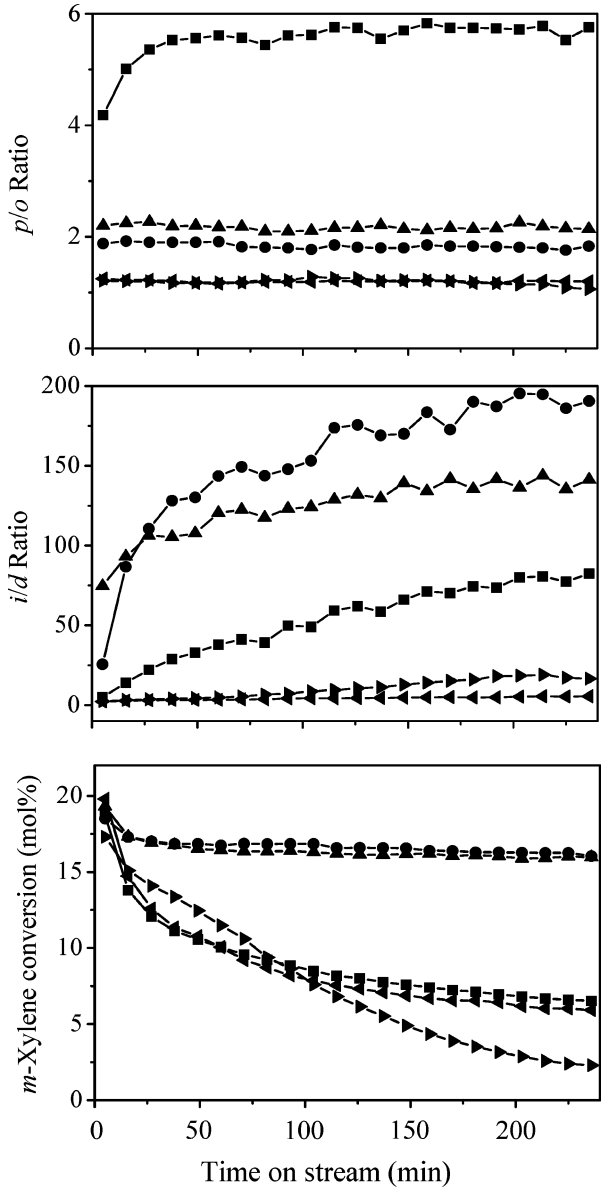

Figure 13. *m*-Xylene conversion (bottom) and *i*/*d* (middle) and *p*/*o* (top) ratios as a function of time on stream in isomerization and disproportionation of *m*-xylene over H-TNU-9 (■), H-ZSM-5 (▲), H-MCM-22 (●), H-mordenite (solid triangle, pointing right), and H-beta (solid triangle, pointing left) at 623 K and 20.3 kPa *m*-xylene pressure.

Figure 13 shows *m*-xylene conversion and *i*/*d* and *p*/*o* ratios as a function of TOS in the transformation of *m*-xylene over H-TNU-9, H-ZSM-5, H-MCM-22, H-mordenite, and H-beta measured under the conditions described above. It can be seen that H-TNU-9 deactivates more rapidly than H-ZSM-5 and H-MCM-22 but no faster than H-mordenite and H-beta. Of particular interest is the observation that, unlike the other four zeolites, H-TNU-9 shows a rapid increase in *p*/*o* ratio at early TOS. Also, its *i*/*d* ratio was found to continuously increase over the period of TOS studied, leading to a negligible formation of undesirable TMBs in the long run. Apparently, these results cannot be explained without considering the positive effect of coke formation on the isomerization activity of TNU-9. After

(27) (a) Olson, D. H.; Haag, *ACS Symp. Ser.* **1984**, *248*, 255. (b) Martens, J. A.; Perez-Pariente, J.; Sastre, E.; Corma, A.; Jacobs, P. A. *Appl. Catal. A* **1988**, *45*, 85. (c) Weitkamp, J.; Ernst, S. *Catal. Today* **1994**, *19*, 107. (d) Corma, A.; Corell, C.; Llopis, F. J.; Martinez, A.; Perez-Pariente, J. *Appl. Catal. A* **1994**, *115*, 121. (e) Guisnet, M.; Gnep, N. S.; Morin, S. *Microporous Mesoporous Mater.* **2000**, *35*−*36*, 47.

240 min on stream for *m*-xylene transformation at 623 K, in fact, H-TNU-9 gave the highest amount (9.5 wt %) of coke deposits among the zeolites employed here (Supporting Information Table 4S). Typically, the rates of coke formation over zeolites containing large cavities with windows of smaller size are higher than those over medium-pore zeolites with 10-ring pores of uniform dimension.[28] Then, suppression of not only the bimolecular disproportionation but also of the less *para* selective isomerization within the 12-ring cavities of H-TNU-9 can be expected after some TOS, giving a rapid increase in both *i*/*d* and *p*/*o* ratios. Although further study is currently underway in our laboratory in order to better understand the shape selective properties of H-TNU-9, we believe that the unique three-dimensional 10-ring pore structure of TNU-9, in combination with its excellent hydrothermal stability, could offer new opportunities for the selective production of a particular class of hydrocarbons, for instance, alkylaromatics.

4. Conclusions

The synthesis, crystal structure, characterization, and catalytic properties of TNU-9, a novel high-silica medium-pore zeolite, have been reported. When the 1,4-bis(*N*-methyl-pyrrolidinium)-butane is used as an organic SDA together with Na^+ ions, TNU-9 was found to rapidly crystallize at the expense of MCM-22(P) over a very narrow oxide composition range. The proposed topology of this new zeolite has been confirmed, and the detailed structure of its as-made form has been satisfactorily refined by combining powder X-ray diffraction and computer simulation techniques. The model for the positioning of organic SDA molecules within the pore network of TNU-9 that is obtained in this way indicates that the same SDA molecule is a close fit for three of the four positions it can occupy in the structure, with one of the sites less favored. Comparison of the catalytic properties in the transformation of toluene and *m*-xylene with those observed with the well-known medium- and large-pore zeolites reveals that TNU-9 with exceptionally high hydrothermal stability could be potentially useful as a shape selective catalyst in many hydrocarbon conversions.

Acknowledgment. Funding for this work was supported by the Korea Science and Engineering Foundation (2006-000-10192-0) and POSTECH (2000538501). We thank S. S. Park (HNU) for technical assistance, Y. K. Park (KRICT) for collection of the variable-temperature IR spectra, and the staff at SNBL, ESRF, for collection of the high-resolution powder X-ray diffraction data. Special thanks are due to L. B. McCusker (ETH), O. Terasaki (Stockholm University), and one reviewer for many helpful comments.

Supporting Information Available: Complete ref 2d and additional information as noted in the text (PDF). This material is available free of charge via the Internet at http://pubs.acs.org.

JA073109G

(28) (a) Chen, N. Y.; Degnan, T. F.; Smith, C. M. *Molecular Transport and Reaction in Zeolites*; VCH: New York, 1994. (b) Karge, H. G. *Stud. Surf. Sci. Catal.* **2001**, *137*, 707. (c) Guisnet, M. *J. Mol. Catal. A* **2002**, *182*−*183*, 367. (d) Lee, S. H.; Shin, C.-H.; Hong, S. B. *J. Catal.* **2004**, *223*, 200.